Cellular processes under mechanical stress: designing an in vitro model for testing burn splinting strategies

APBC

TUDelft

Thesis manuscript

Cellular processes under mechanical stress: designing an in vitro model for testing burn splinting strategies

By

Yoni de Jong
4730313

Master Thesis Biomedical Engineering (BM51032)

Department of Biomedical Engineering,
Faculty of Mechanical, Maritime and Material Engineering,
Delft University of Technology
And
Association of Dutch Burn Centers Laboratory

To be defended on September 26th, 2019

Thesis Committee:

Ludo van Haasterecht	VU Amsterdam, daily supervisor
Prof. dr. ir. H. H. Weinans	TU Delft, supervisor
Dr. Shahram Janbaz	TU Delft
Dr. J.J. van den Dobbelsteen	TU Delft

Table of contents

Abstract

Introduction. To prevent burns from scar formation and contraction, the use of splinting therapy in the early phase of wound healing is considered as an effective non-surgical method. Splinting entails the application of a mechanical load in the opposite direction of the contractile force within the wound, based on the assumption that wound- or scar contraction will be prevented or reduced. However, clinical research provides conflicting evidence on its effectiveness and optimal treatment method. Therefore, the aim of this study was to design an in vitro model to investigate the mechanoresponsive cellular effects of stress on specifically Human Eschar Fibroblasts and their extracellular matrix, in order to confirm or disprove effects of burn splinting.

Methods. The two major players of the burn wound model include (1) the fibroblasts, and (2) the novel extracellular matrix they produce. Outcome measures were chosen that directly relate to matrix organization, fibroblast functioning and matrix functioning. Three chronological sub-goals were defined to achieve the goal of designing a burn wound splinting model: (1) Formulating a suitable mechanical stress protocol; (2) Select a system that enables the selected mechanical stress of extensible substrates that facilitate the growth of fibroblasts and their derived extracellular matrix; (3) Create and optimize conditions to culture fibroblasts on an extensible substrate. To successfully reach these goals, the current literature on this subject was evaluated and comparative experiments were executed. Feasibility of the model was tested in a pilot study.

Results. The MCB1 stretching apparatus was provided by Association of Dutch Burn Centre as a suitable device, which was modified to fulfill all predefined requirements. Human Eschar fibroblasts and dermal fibroblasts were cultured on custom made silicone culture wells. Cross-linked gelatin-A coating and vitamin C-supplemented culture medium were selected for optimal cell culturing results. A clinically relevant stretching regimen was chosen, given the paucity of available evidence in literature. A pilot study to test the feasibility of the model indicated that both dynamic and static stretching of eschar fibroblasts show a trend towards thicker, denser collagen matrices compared to unstretched conditions. These collagen fibers also showed a greater degree of alignment. However, no definitive conclusions can be drawn since sample size is limited.

Conclusion. The model presented in this work constitutes a practical framework to test mechanotransducive processes in burn scars on a cellular and molecular level. A pilot study using this model showed excellent feasibility

Keywords: burns, rehabilitation, humans, skin, splinting, stretching, mechanical load, mechanotransduction, collagen, (myo)fibroblasts, scar, wound healing, contraction

1. Introduction

A burn is a partial or complete destruction of the skin caused by heat, electricity, chemicals or radiation. In 2011, in the Netherlands an annual number of 747 people suffered from serious burn injuries for which treatment was needed and whom were admitted to hospitalizations at one of the three Dutch burn centers in Beverwijk, Rotterdam or Groningen[1]. Patients suffer from long-term physical dysfunction and psychological harm from the scars. Furthermore, studies demonstrate a prevalence of 38-54% for burn scar contractures that are the pathological outcome of excessive scarring and ongoing scar contraction (see Figure 1)[2,3]. Scar contractures can expand to underlying connective tissue and muscles, resulting in limitation in joint range of motion and participation of daily activities. Scar contractures do not subside, although they may improve with time with occupational therapy or physiotherapeutic treatment and physiotherapy. A comprehensive rehabilitation program is essential to decrease these post-traumatic effects and improve functional independence[4–7].

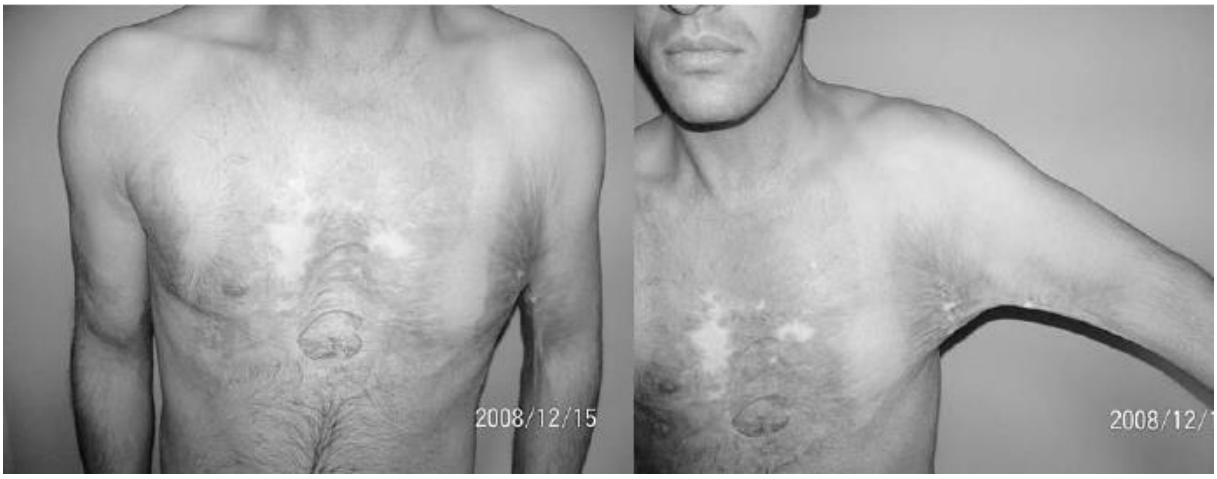

Figure 1. Mature burn scar involving almost entire anterior chest and scar contracture at shoulder. Reproduced from Nisanci M. et al. (2014)[8]

1.1 Human skin

Human skin can be divided into three layers based on anatomy and functionality: the epidermis, dermis, and subcutis[9].

The outer layer, the epidermis, serves as protection against mechanical, chemical and biological damage. Epithelial cells line the outer surface of the skin.

The layer directly underneath epidermis is called the dermis. The limited cellular component of the dermis consists of mainly human dermal fibroblasts (HDF), housekeeping cells of the dense network of extracellular matrix (ECM), see figure 2. The structural integrity of human skin is largely dependent on the quality of this ECM, which is produced, organized, and maintained by HDF[9]. The ECM consists of fibrous proteins, proteoglycans, and minerals. Proteoglycans are molecules that consist of a "core protein" with one or more covalently attached glycosaminoglycan chains. Fibrous proteins include a range of collagens, which provide strength and resilience helps give structure and mechanical support.

Next to collagens, fibrous proteins include elastin, responsible for the skin's elastic properties. The core protein of a proteoglycan can interact with collagen fibers at specific sites, and these interactions are important in maintaining the overall structural organization of the ECM[10]. Here integrin transmembrane receptors serve as transmitting outside-in and inside-out signals from the cell to the ECM and in reverse, to mediate cell survival, proliferation and motility. Changes due to mechanical tension leads to the clustering of integrins into macromolecular structures, termed focal adhesions and other types of cell-matrix adhesions. These adhesions are signaling proteins that serve as link between integrin receptors and actinmicrofilaments inside the cell. This provides the mechanical link through which cellular forces are transmitted to and from the extracellular environment to the intracellular cytoskeleton[11,12]. The interaction between cells and ECM assists in maintaining normal cellular physiological activities, in addition to playing an important function in multiple pathological processes, including wound healing, scar formation, and tissue fibrosis[11].

The dermis is organized into two regions based on differences in ECM concentration and cell alignment. The most superficial layer, the papillary dermis, is approximately twice the thickness of the epidermis and is composed of especially parallel oriented loose, thin collagen type III fibers and elastic fibers. The bulk of the lower dermis, the reticular layer, contains especially randomly oriented large, loosely interwoven collagen type I bundles[13].

The third inner layer, the subcutis or connective tissue layer, mainly serves as storage of fat[9].

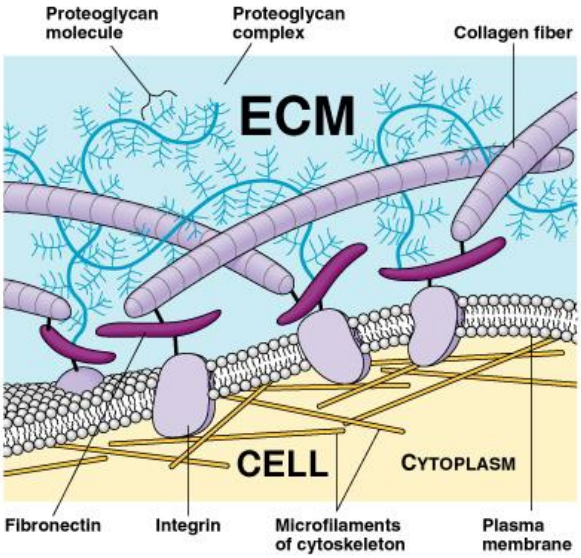

Figure 2. Schematic representation of the interaction between a cell and its surrounding ECM including proteoglycans and collagen fibers. Reproduced from Couet J. et al. 1997[10].

1.2 Skin burns

In the case of a deep burn (i.e. deeper than the epidermis), the dermis is affected, resulting in dead cells and denatured connective tissue. Denaturing means the loss of the spatial structure of whereby properties and functioning often change considerably[14]. In the wound, these affected cells and connective tissue are present at the surface, called 'eschar'[14,15]. It usually has a discolored or even black

appearance. Although this eschar sloughs off after weeks to months, it is usually removed earlier if it interferes with the underlying wound healing[14]. In this eschar tissue, some viable human eschar fibroblasts (HEF) are found, depending on wound depth[16].
Unlike fetuses and rodent species, humans do not have regenerative capacity in the skin and only repair takes place. This 'reparation of the skin' displays wound healing by fibrosis and scar formation, whereas 'regeneration of the skin' displays complete substitution of the tissue[17]. In order to repair and close the wound, the wound healing process starts. Wound healing is a complex but highly organized process, in which healing typically occurs through a complex cascade of biochemical and cellular events in four general overlapping phases: hemostasis, inflammation, proliferation, and remodeling. All these stages are present in burn injuries, although the timescale of each stage differs depending on the severity of the burn wound[6].

Hemostasis is the process of bleeding stopping by clotting processes. After blood vessel constriction, platelets adhere to the surface and fibrin strands begin to create a mesh resulting in a clot. Inflammation begins after injury when blood vessels leak transudate (made of water, salt and protein) causing localized swelling. Proteases such as matrix metalloproteases are attracted to the wound during the inflammatory phase and have an important role in breaking down damaged ECM to make room for new tissue formation. Macrophages and neutrophils remove dead cells, which triggers release of proinflammatory signals such as transforming growth-factor beta-1 (TGFB1)[18]. Proinflammatory fibroblasts start to produce ECM to repair the skin, which is the start of the proliferative phase[18]. TGFB1-stimulation leads to proliferation of fibroblasts and their differentiation into a pro-fibrotic fibroblast type: the myofibroblast. Myofibroblasts produce high amounts of ECM (mainly collagen) and cytokines[19]. These components mainly consists of type III collagen and fibronectin[4,6,19,20]. Next to this, myofibroblasts develop a muscle-like contractile apparatus composed of stress fibers which are actomyosin bundles. Actomyosin bundles consists of actin and myosin held together by cross-bridges. By sliding past one another, this interaction between actin and myosin leads to the myofibroblasts having contractile capabilities[7] . Myosin and actin within these stress fibers are linked to the earlier mentioned focal adhesions[21], which serve as macromolecular complex that links the intracellular cytoskeleton structurally with the ECM. Because of this mechanical connectivity, activated myofibroblasts cause contraction of the ECM and corresponding closure of the wound. These capabilities are necessary for wound closure during the wound healing process[4,6,20], which is essential during the first stages of wound healing to avoid contamination as much as possible.
Later, during maturation, type III collagen is replaced by type I collagen. Originally disorganized collagen fibers are rearranged, cross-linked, and aligned along stress lines. The provisional matrix is replaced with an ECM that more closely resembles ECM found in non-injured tissue, interlaced by type I collagen and type III collagen changing their ratio from 1:4 to 1:2[18,19].

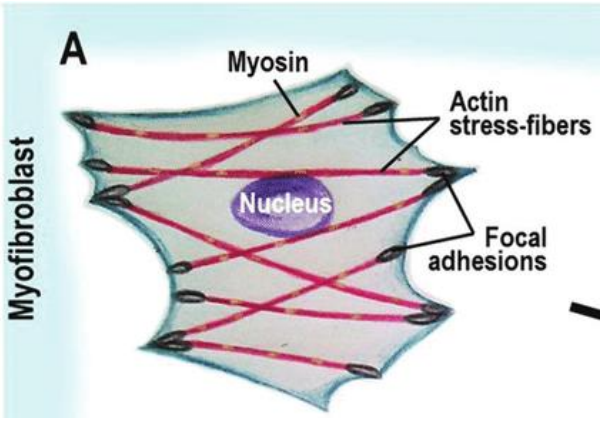

Figure 3. Schematic representation of the myofibroblast. These contractile fibroblasts are characterized by the formation of myosin-containing actin contractile stress fibers. Reproduced from Bildyug (2016)[22].

At the end of the normal wound healing process, the ECM is reconstituted and epithelial cells resurface the injury. Cells that have served their purpose during wound healing, like myofibroblasts, are removed by programmed cell death or apoptosis, and their contractile and synthesizing activity is terminated[2,4].

1.3 Scarring

In situations in which normal wound healing fails, and this process continue after wound closure, scar contraction can occur. This is seen in situations where myofibroblast activity persists in the wound bed after wound closure, causing a fibrotic environment in which enhanced contraction, excessive ECM formation and cytokine secretion is generated. Fibrotic tissue is stiffer than healthy skin and contains high levels of TGFB1. Since myofibroblast differentiation is induced by TGFB1 in conjunction with matrix stiffness, the fibrotic environment stimulates myofibroblast differentiation and persistence[3,7]and thus further induce a fibrotic environment, leading to a vicious circle. Although these wound healing processes are necessary in moderation to close the wound during the first stages of wound healing, continuation of these processes after wound closure results in irreversible accumulation of collagen and contraction of the collagen matrix[23,24]. This ongoing process leads to hypertrophic scarring (thickened, wide, often raised scar) and scar contraction.

Histological differences in collagen between healthy skin, normotrophic scars, hypertrophic scars, and keloid scars can be found in table 1. As can be seen in this table, organization of collagen fibers and synthesis characterize these different skin tissues in terms of for example collagen alignment, matrix density and synthesis. For example, scarring, especially hypertrophic scarring, involves aberrations in matrix deposition[13]. Both the total amount and organization of the newly deposited ECM will differ from healthy skin; increased volume of well-aligned collagen fibers are found in cutaneous scars. In addition, higher a-SMA gene expression rates are measured in normotrophic and hypertrophic scars compared to the unwounded skin. An important factor influencing scar quality is healing time, in particular epithelialization time[25].

	Unwounded skin	Normotrophic scar	Hypertrophic scar	Keloid scar
Collagen fiber alignment	Basket weave-like network Parallel to epidermis	Fine, well-organized Parallel to epidermis	Flatter, arranged in a wavy pattern Predominantly parallel	Collagen I and II fibers lie haphazardly Randomly oriented
Collagen bundle thickness	Normal bundle	Small, parallel bundles	Thin collagen, thin fibers organized into nodules	Large, thick, closely packed random to epidermis
Collagen matrix density	Smaller bundle distance	Close	Close	Larger bundle distance
Collagen synthesis	Normal	Increased than normal	Seven times higher than normal	20 times higher than normal
Collagen I/III ratio	5:1	6:1	6:1	17:1
a-SMA gene expression rate	Normal	Increased than in normal	A lot higher than normal	Decreased than in normal

Table 1. The histological differences in collagen between normal, hypertrophic, and keloid scars. Modified from Verhaegen et al. (2009)[13].

1.4 Splinting

When the injured site is over a highly moveable positions of the body such as joint surface, additional precautions should be taken to reduce scar contractures. Currently, the most common non-operative method to treat and prevent contractures is splinting[26,27]. A splint is defined as “a rigid or flexible device that maintains in position a displaced or movable part; also to keep in place and protect an injured part’[28]. A well-designed splinting program incorporated with passive and/or active mobilization is essential to prevent or reduce joint contractures and deformities. Common splinting treatments are either “static splinting”, in which the burn injury is braced in a fixed position to apply torque to a joint in order to statically position it as close to end range as possible, or “dynamic splinting”, a combination of static splinting with range-of-motion exercises (Figure 4a and 4b).

The use of splinting during wound healing or on mature scars is inspired by the concept of ’mechanotherapy’ underpinning how load may be used therapeutically to stimulate tissue repair and remodeling and to maintain functionality and range of motion. It is based on the assumption that wound- or scar contracture will be prevented, reduced or stopped by applying a mechanical load in the opposite direction of the contractile force within the wound caused by the myofibroblast activity[4,27] (Figure 4c).

Splints are not only essential for positioning and prevention of contractures, but also for stretching and lengthening of already contracted scar tissue to correct the scar contracture[4,27]. If the condition of the skin permits it, and/or pain can be tolerated, static splint should be serially adjusted to counteract the contracture as much as possible[4,27]. Therefore, splinting techniques are often related to the concept of applying stretch to the wounds.

(a)

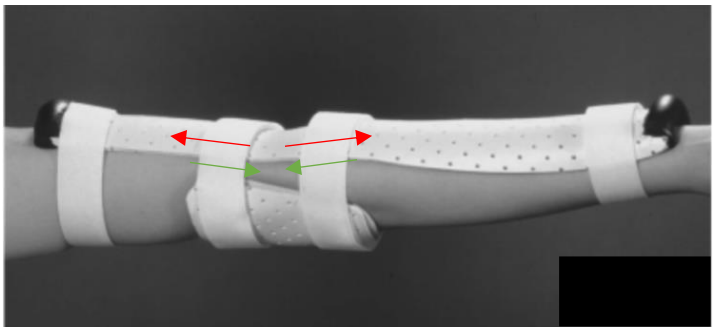

(b)

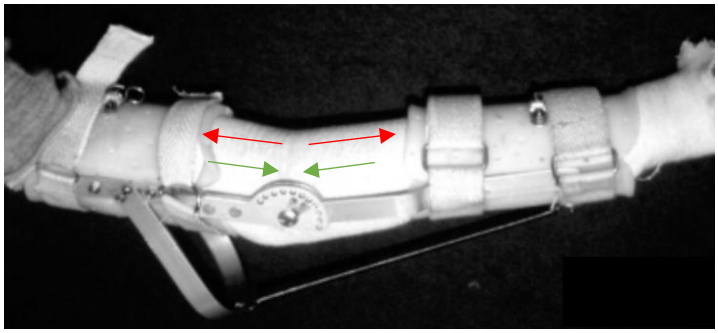

(c)

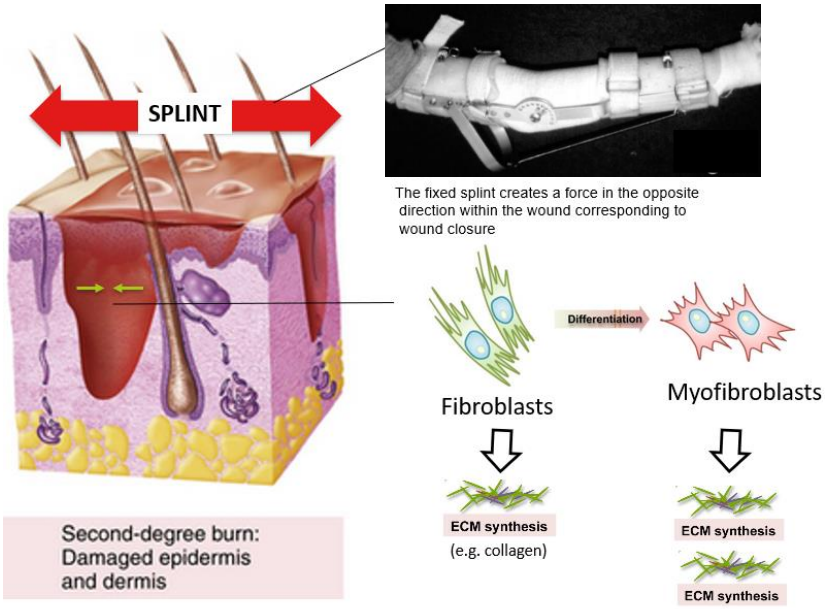

Figure 4. Clinical example of static and dynamic splints used in the prevention of scar contractures in the elbow pit. (a) Volar approach static elbow extension splint where mechanical load (red arrows) is applied in the opposite direction of the contractile force within the wound caused by myofibroblast collagen matrix contraction (green arrows). (b) Dynamic elbow brace with extension device. (c) Derailment of wound healing in case of second-degree burn and application of splinting method. Reproduced and modified from Kwan et al. (2002)[29] and Patton et al. (2014)[30].

Splinting of the burns and/or contracture is considered an effective non-surgical method adopted for scar management, as multiple studies have reported an improvement in range of motion and functionality[3,26,31–33]. However, clinical research provides conflicting evidence on its effectiveness and optimal treatment method. Strong evidence from large prospective randomized trials is lacking[4,6]. Such trials are necessary to properly compare the different methods of splinting, yet differences in burn wound etiology, treatment protocols and patient compliance make the comparison of such studies difficult[4,32].

In addition, since scar contractures are often seen around joints, a place where high mechanical loads to the skin are seen due to movement, it is insinuated that mechanical loads stimulate the formation of scars and contractures instead of reducing this[7]. This indicates that loads caused by splinting therapy may even counteract its own purpose and would promote scar formation and contractures. Following this rationale, therapies should focus on reducing mechanical forces in the wound environment instead of counteracting them, which seems contradictory to the action of applying splints to healing wounds. Clearly, no consensus currently exists on the efficacy of burn splinting.

2. Formulating the research goal

Further research is needed to investigate the influence of mechanical stress on burn wounds and healing processes. Clinical research is limited by patient numbers and ethical considerations. Using a scientific model to investigate the effects of splinting circumvents these ethical restraints, and allows the elucidation of underlying disease mechanisms not apparent in purely clinical research. Several scientific models can be used, their advantages and disadvantages will be discussed here.

2.1 Experimental scientific models

Animal testing is an often-described technique in burns research. The extent to which animal testing can be translated to humans is dubious[33]. Ethical considerations further limit the use of animal models. In fact, the Association of Dutch Burn Centre (ADBC) is one of the pioneers in the Dutch scientific community in the complete abolition of animal testing. Consequently, all research funded by the ADBC shall absolve from using animal models.

Another option is to use ex vivo tissue to investigate the cellular and matrix changes in burns due to mechanical loads[33]. Ex-vivo refers to experimentation or measurements done on tissue from an organism in an external environment with minimal alteration of natural condition. In ex-vivo experiments complete skin tissue samples from humans can be used for experimentation in an external environment, outside the human body. In practice, this involves surgical waste material from interventions where excesses of skin are removed from a patient and pathological evaluation is not needed. This seems desirable as it provides minimal alteration of physiological conditions and as such is close to the clinical situation. It is, however, difficult to control those conditions that differ from the clinical situation: this model excludes the systemic variables circulation, nutrition through blood flow, and the inflammatory response[33]. It is therefore hard to accurately mimic the pathological conditions of hypertrophic scarring and wound healing[33].

An alternative research method that is described by Frohlich et al. (2014) is the use of in vitro studies. An in vitro study means that experiments are performed with molecules or cells outside their normal biological context in cell cultures[33]. Using this technique, a scientific model preferentially consists of only the elements that play a significant role in the disease process, simulating a simplified version of a complex biological phenomenon. The principal elements in the case of hypertrophic scarring are the fibroblast, the surrounding matrix, and the inflammatory response. These can be simulated using in vitro models. Fibroblasts can be derived from different tissues, such as skin, pathological scars and burn wounds. Investigating fibroblast as a separate entity does not suffice however, as the interactions between cells and matrix is of utmost importance; the cell-matrix complex should be considered as a whole. To create a model to assess the effect of splinting on burn wounds, both cells and matrix have to be included. The concept of engineering three-dimensional fibroblast-derived ECM constructs is frequently used in dermatological research. Since fibroblast secrete and organize ECM, the basic approach is to allow fibroblasts to produce their own three-dimensional ECM while attached to a culture surface. The matrix closely resemble in vivo mesenchymal matrices. Utilizing in vivo-like three-

dimensional matrices allows the acquisition of information that is physiologically relevant for characterization and measurements of cellular responses to the three-dimensional matrix microenvironment[34]. Furthermore, to this model, mechanical stimulation can be applied as intervention. Mechanical stimulation of these variables in culture allows the simulation of splinting in the early wound healing phase in vitro[31,35,36] In this type of experiments mechanical stress is applied to the fibroblasts while they proliferate and produce novel ECM in vitro. It provides an simplification where controlled dosing of mechanical stress directly influences the behavior of cell, as seen by alterations in the subsequently produced matrix structures.

A major advantage of using fibroblast derived three-dimensional ECM, is that it allows us to directly observe the effect that mechanical stimulation has on changes in matrix properties like organization and stiffness. It provides a more reliable outcome measure, compared to cell-focused outcome measures as the matrix ultimately is responsible for scar contracture[37]. Additionally using cell cultures provides consistency and reproducibility of results that can be obtained from using a batch of clonal cells. As this is a simplification of the clinical situation, and systemic variables are missing we must be refrain from direct extrapolation of results obtained from in vitro experiments to the clinical situation[33].

2.2 Current knowledge on in vitro studies

When analyzing previous in vitro studies during my systematic literature study, in these experiments relationship between mechanical stress, in the form of stretch, and functional unit (cell and matrix) were investigated[17,19–37]. The concept of engineering fibroblast derived three-dimensional ECM was applied in which fibroblasts were seeded onto flexible substrates where on mechanical stretch was applied with help of stretch devices. Here, the influence of mechanical stretch was determined by outcome measurements on fibroblast alignment and ECM formation in terms of collagen deposition and histology, but also myofibroblast expression rates. Studies indicated that human fibroblasts subjected to mechanical stretch, altered its structure and properties resulting in induced myofibroblast differentiation and excessive collagen production. These effects have a strong similarity to mechanisms seen during wound healing process where scar formation occurs. Consequently, this suggests that application of mechanical load on skin, wounds or scars might promote scar formation and contraction, instead of reducing it.

However, study designs along the literature research showed great heterogeneity: The studies used a range of different apparatuses were used for the application of mechanical. These differed in stretch dimension (biaxial, uniaxial), stretch regime (static, dynamic), stretch, frequency and duration. Therefore, drawing conclusions about the outcome results have to be done carefully. Additionally in included studies little research has been done on the magnitude of the stretch set to the stretch apparatus and the stretch that is actually performed to the flexible substrates on which the cells are growing. In the studies the cells attached on the silicone sheet are expected to experience the same deformation as the silicone sheet itself, while this might deviate. For example, in the study of Balestrini et al. (2006), using FX-4000 apparatus, deformation occurs by using vacuum pressure at the edges to stretch a circular silicone substrate over a fixed loading post. Here, stretch at the edge of the sheet is

larger and gradually decreases towards the center. Next to that, the mechanical stimuli experienced by cells attached atop the substrate include not only substrate elongation, but also potentially confounding reactive fluid stresses due to coupled motions of the overlying liquid culture nutrient medium[56]. This has great effects on results related to specific strain rates in this review.

Cell types used in these articles were fibroblasts derived from healthy skin (HDF), hypertrophic scars (HF) or keloids (KF). Research on the mechanoresponsive cellular effects of stretch on fibroblasts derived from burn wound tissue (HEF) was absent: HEF are fibroblasts that are active in wound healing process in burns and are thought to be the key players in the onset of hypertrophic scarring and scar contraction in these wounds. HEF support wound healing directly by secreting collagen types I and III. They can also indirectly affect the healing response by inducing myofibroblast activation and matrix protein remodeling. Consistent with this, HEF are not detected in non-injured skin[16].
Research on the effect of mechanical stress on these specific cells and their ECM will provide a molecular basis confirming or disproving the effects of burn splinting.

The aim of this thesis was therefore, to design an in vitro model of mechanotransduction in burn wounds, to investigate the molecular effects of burn splinting in vitro.

2.3 Model definition of 'burn wound splinting'

The major elements of the in vitro burn wound model are (1) fibroblasts derived from burn wounds and fibroblasts derived from healthy skin to compare physiological situation with a pathological situation, and (2) the fibroblast derived ECM. Minor factors include the culturing media and growth-promoting substrates. The splinting model consists of mechanical force which is applied to the burn wound model. The set-up will apply a pre-defined stretching regimen to the culture system. To transmit the mechanical stress from the mechanical device to the fibroblasts, fibroblasts will have to be seeded on an extensible substrate, allowing the cells to sense the applied forces

To come up with a model that mimics burn wound splinting, outcome measures had to be set. Furthermore, three chronological sub-goals were defined to achieve the goal of designing a burn wound splinting model:

(1) Formulating a suitable mechanical stress protocol
(2) Select a system that enables mechanical stress of extensible substrates that facilitate the growth of fibroblasts and their derived ECM
(3) Create and optimize conditions to culture fibroblasts on an extensible substrate

3. Methods

The goal of this project was to design a model to investigate the effect of mechanical stress on dermal burn wounds by applying mechanical stress to fibroblasts and their derived matrix in vitro. The model can therefore be split into the burn wound part, and the subsequent splinting part.

Based on selection of measurements and sub goals, a research framework was designed (visualized in Figure 5). The model was eventually tested in a pilot experiment in which the model functioning was validated.

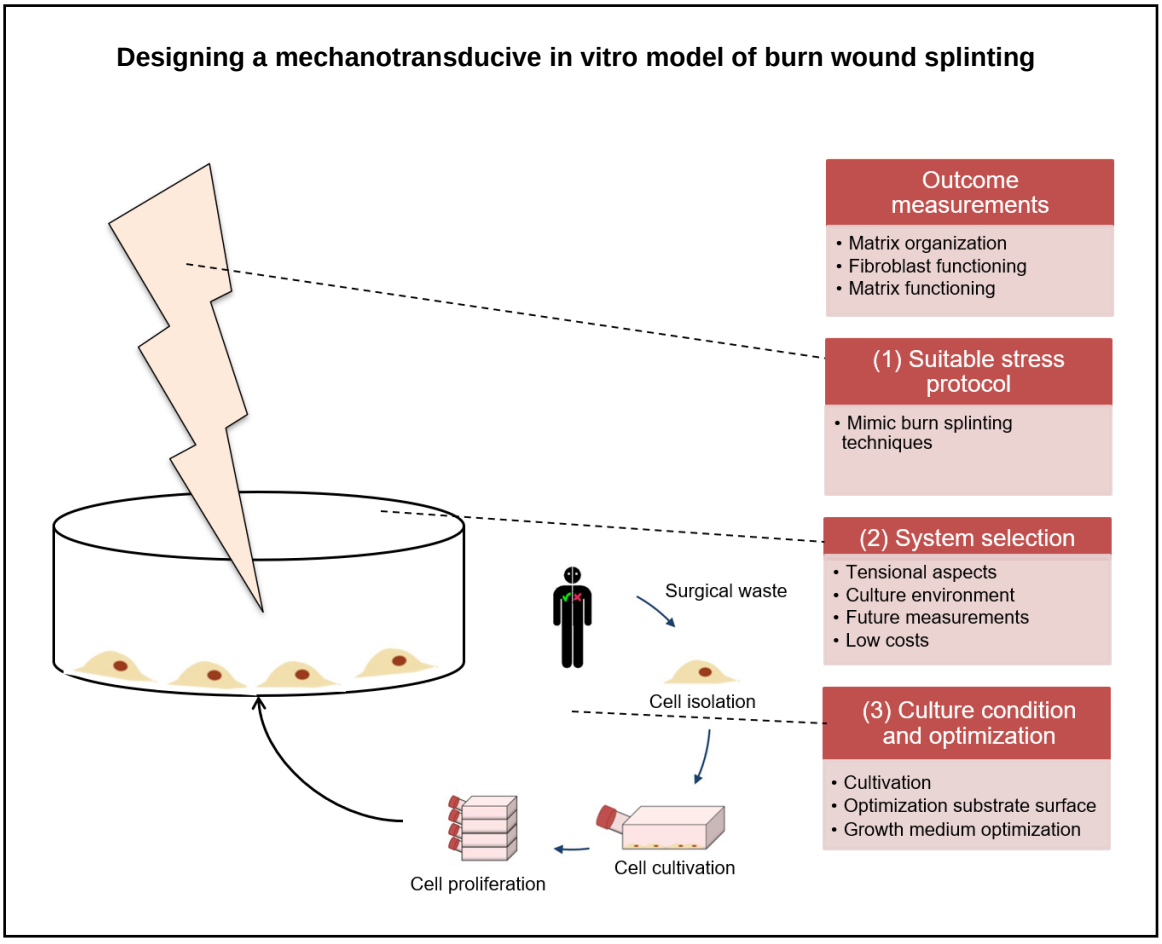

Figure 5. Research framework

3.1 Outcome measures

As specified earlier, the two major players of the burn wound model include (1) the fibroblasts, and (2) the novel ECM they produce. As a scientific model is a simplification of the actual physiological situation, careful attention should be paid to the selection of outcome measures and criteria. Using outcome measures that are relevant to the physiological situation make the results of in vitro research more translatable, improving the impact of the experiment. For this reason, outcome measures were chosen that directly relate to matrix organization (i.e. nonlinear microscopy imaging techniques and immunohistochemistry), fibroblast functioning (i.e. gene expression assays), and matrix functioning (i.e. stiffness analysis). Matrix organization measurements can be achieved in terms of collagen fiber alignment and synthesis. Outcome measurements can be related to tissue quality and characteristics of scarring.

3.1.1 Matrix organization

Collagen can be visualized using a variety of imaging techniques including bright-field microscopy, polarized light microscopy, immunohistochemistry, and second-harmonic generation (SHG) microscopy[57]. A great disadvantage of using immunohistochemistry staining is its reliance on histological sections. Fixation, embedding, and cutting of these sections involves significant manipulation of samples, potentially influencing outcomes. Its also a time consuming and laborious technique[44]. Confocal reflectance microscopy and optical coherence tomography (OCT) can provide three-dimensional visualization of bioengineered dermal skin samples without having to process the samples[58]. However, they lack specificity as their contrast mechanism relies on spatial variations in refractive indices. Three-dimensional interactions between cells and collagen fibers cannot therefore be studied using this type of contrast mechanism. For that, exogenous fluorescent markers or fluorescent fusion proteins are used to specifically detect the cells or to mark their surrounding environment, requiring sample processing. Ideally we would use highly specific three-dimensional in situ imaging methodologies that enable simultaneous monitoring of the three-dimensional collagen network and of the fibroblast distribution in unstained and unprocessed samples. Multiphoton microscopy offers this three-dimensional multimodal imaging capability, as it provides structural and molecular contrast in unstained samples which is impossible when using other noninvasive methods[59]. However, there exists a great need to easily and robustly quantify images from these modalities for individual fibers in specified regions of interest. Recent advances in the imaging of fiberlar collagen using SHG imaging in combination with two photon excitation microscopy have proven useful in enhancing our understanding of the supramolecular changes that occur in scar formation and dermatological diseases[60].

3.1.1.1 Non-linear microscopy

SHG microscopy has emerged as a powerful three-dimensional imaging tool for studying biological processes in unprocessed and unstained samples[60].

The use of SHG microscopy in dermatological research has seen an enormous increase in the past years. This optical technique involves two photons interacting within a nonlinear structure of the selected sample, resulting in a single photon with half the wavelength and twice the energy[60]. The second order

non-linear susceptibility of a structure is dependent on its internal symmetry, and in the case for fiberlar collagens this susceptibility provides excellent molecular contrast. Type I and II collagen are fiberlar proteins with a non-centrosymmetric triple helical structure that provides SHG signals under the right conditions. The technique thus provides high-resolution images of non-processed samples in three dimensions. The underlying optical process differs from fluorescence in the sense that no excitation of fluorophores takes place, and thus no photobleaching occurs in SHG. As this is a two-photon process, it only occurs at the point where the collimated light of a powerful laser is tightly focused resulting in a tiny focal point and excellent spatial resolution. The spatial resolution for this system is around 0,5 um, while the axial resolution is about 2 um. Images are made by line-scanning a two-dimensional surface in the sample. Three-dimensional imaging is performed by sequentially recording these images along a range of depth. Reconstruction of such a stack of images results in a three-dimensional 'z-stack'. Penetration into dense tissue can easily be achieved up to 100 um[57].

SHG can be used independently or in conjunction with other imaging techniques - such as Third Harmonic Generation or Two Photon Excited Fluorescence (2PEF)[57,60]. 2PEF involves two photons arriving simultaneously at a fluorophore; contrary to SHG where the molecule is excited to a virtual state, the fluorophore is excited in 2PEF and energy transfer takes place. It has advantages similar to SHG, and with appropriate spectral filters, the two techniques can be combined to provide multi-modal imaging[61]. Most fluorescent probes can be excited with 2PEF, yet the existence of naturally present fluorophores in biological tissue makes this an extremely useful technique to use in unprocessed tissue. In the case of cell cultures, convenient fluorophores include NADP(H) and FAD(H), as important redox agents in the cellular metabolism[57].

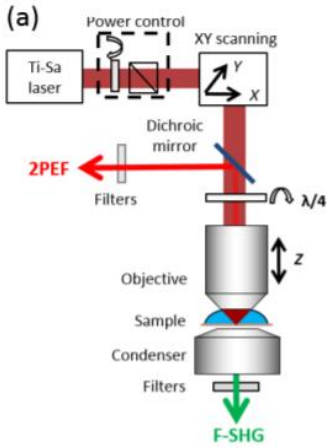

Figure 6. Combined SHG and 2PEF microscopy set-up. Reproduced from Bancelin et al. (2014)[62].

The setup for SHG and 2PEF imaging can be seen in figure 6 and includes a Ti-Sapphire femtosecond oscillator (Coherent Chameleon Ultra II), using an 80 MHz repetition rate. An 800 nm laser bundle is focused on the sample using a commercial laser scanning microscope (TrimScope 1, Lavision BioTec). A high-NA objective (Nikon APO 25×/1.10) is used to focus the light on the sample. The epi-generated signal is split and detected by a set of photomultiplier tubes (Hamamatsu).

Image processing was done using ImageJ (Version 1.52a for windows) and curve Align software for quantitative analysis of collagen fiber alignment and synthesis.

3.1.1.1.1 Quantitative analysis of collagen synthesis and density

Determining collagen density in the samples is important as increased collagen density has been described in pathological scars, as mentioned earlier. For example, as can be seen in table 1, excessive collagen synthesis and higher density is seen in scars compared to normal unwounded tissue.

To quantify collagen synthesis, three-dimensional images from collagen fibers were first retrieved in combined SHG/2PEF z-stacks, with 2-um z-step. At the regions of interest collagen synthesis was related to the collagen matrix thickness of the samples. Therefore, at this region of interest the collagen matrix thickness was determined by counting the slices of z-stack showing collagen[61].

For quantification of collagen density, selected ROIs were processed using macros developed with ImageJ to obtain the volume occupied by the thresholded SHG image z-stack. SHG images were thus converted to binary images based on adaptive thresholding, and the collagen density was obtained as the area percentage of voxels of the corrected SHG mask

3.1.1.1.2 Quantitative analysis of collagen fiber alignment

Specific changes in collagen alignment play an important role in contributing to the mechanical properties of tissues and are associated with disease progression[60]. As summarized in table 1, collagen fiber alignment shows changes in diseases states. In essence, instead of a random basket weave formation of the collagen fibers found in normal unwounded tissue, collagen aligns in a direction parallel to the skin in scar tissue[63]. The analysis of fiber alignment can be done with a range of image processing techniques that are generally based on the intensity derivatives or intensity variation, Fourier transform or Hough transform or directional filters, or fiber tracking algorithm. Currently freely available open-source software tools for collagen alignment quantification include the ImageJ plug-ins “FiberTool” and “Alignment J”, the MATLAB (MathWorks, Natick, MA, USA) stand-alone applications “CytoSpectre”, “CurveAlign”, and “CT-FIRE”[64].

Here, we describe the latest version of CurveAlign (CA, CurveAlign 4.0), which provides a powerful and comprehensive platform for quantifying fiberlar collagen on a global, region of interest (ROI), and fiber basis. CurveAlign is a quantitative tool that calculates global and localized collagen features including angle, alignment, and density. Alignment of fibers is calculated with respect to each fiber or fiber segments. This alignment coefficient is thus a measure of local organization of parallelism. The alignment coefficient ranges from 0 to 1, with 1 indicating perfectly aligned fibers, and smaller values representing more randomly distributed fibers[64]. This technique has been successfully used in numerous studies of collagen alignment. For example, CA-based orientation analysis was used in SHG images acquired from human pancreatic histology tissues, and to quantify collagen alignment in breast cancer tissue where it indicated significantly less aligned fibers after treatment of a tumor[64].

3.1.1.2 Immunohistochemistry

Although SHG imaging helps to quantity directionality and density of fiberlar collagen, it is very specific for type I and II collagen meaning that other types that are potentially of importance such as type III will not be picked up with this technique[60,62]. Also for example myofibroblasts can be detected by immunostaining. As can be seen in table 1, the ratio of collagen type I/III and presence of myofibroblasts is a marker for pathological scars, and thus might be an interesting outcome measure in a burn wound model.

Immunohistochemistry is a method for demonstrating the presence and location of proteins in tissue sections. Immunostaining allows for the selective visualization of ECM molecules, cellular receptors, and intracellular proteins using primary antibodies to bind to a target molecule. It is used in cell biology to study differential protein expression, localization and distribution at the tissue, cellular, and subcellular level[65].

To detect collagen-I fibers and myofibroblast cells, double immunostaining can be applied on the samples. Cell medium is removed from the cell cultures and cells are rinsed with 0.1M phosphate buffered saline (PBS). Cells are then fixed in 4% formaldehyde. Following a rinse with PBS, the non specific binding sites are blocked with 10mg/mL of bovine serum albumin in PBS containing 1mg/mL glycine for 30 min. Unbound primary antibodies are removed by rinsing followed by incubation with the preformed primary–secondary antibody complex against the second antigen for 1h.
The preformed primary-secondary antibody are created by mixing primary, Mouse-anti-human alpha smooth muscle actin or mouse-anti-human collagen1 together with secondary antibody, rabbit-anti-mouse biotin, together in a test tube and incubate in the dark for 1 h. Excess secondary antibodies not conjugated to the primary antibody are quenched by adding a predetermined concentration of IgG from murine serum, which is added to the preformed complex and incubated for a further 1h. The performed primary secondary antibody mixture is then incubated with the cells for 3 h. Optimal concentrations of primary and secondary antibodies are set to 1:500 and 1:300 respectively and 1:500 green-fluorescent Streptavidin-AF488 and red-fluorescent Streptavidin-AF647PE. In single immunostaining cells can be visualized using DAPI.

Samples are imaged with Axioskop 40 FL (Zeiss). Streptavidin-AF488 labeled samples are imaged using the FITC filter, and Streptavidin-AF647PE using the Texas Red (TXR) filter. Images are saved as 8-bit greyscale images and then processed for merging, which involved digitally applying a color map for each filter (green for col3 and red for a-SMA). Both colored images are then merged using image-matching software.

3.1.2 Fibroblast functioning

As mentioned earlier, myofibroblasts have been implicated in the pathogenesis of tissue fibrosis and hypertrophic scarring[21]. It has been shown that in vitro cultured fibroblasts are able to differentiate into

myofibroblasts which actively participate in the production of a fibrotic environment. The differentiation into myofibroblasts is caused by changes in gene expression. Gene expression controls the amount and type of proteins that are expressed in a cell and shows its activity at any given point in time[21,41]. Therefore, it is valuable to obtain information about the myofibroblast marker a-SMA gene expression rates, and the effect of mechanical stress on these rates.

3.1.2.1 Gene expression rate

The degree of a-SMA expression is related to fibrosis and fibroblast contractile activity as seen in a study of Hinz et al. (2001)[66]. By quantifying gene expression rates of a-SMA before and after mechanical stimulation, we are able to measure the mechanotransducive effect of stress in the cell's surrounding, down to cell nucleus[31].

In addition, myofibroblast activity is known to increase in response to mechanical strain and stimulate collagen production[21]. By also determining the activity of ECM-related genes like Col1a and Col3, we have another measure of quantifying the prolific nature of the fibroblast subtype.

Quantitative Real-time polymerase chain reaction (q-PCR)

Determination of expression rates can be done with help of RNA isolation, cDNA transcriptase and Quantitative polymerase chain reaction (qPCR) analysis. PCR allows isolation of DNA fragments from DNA by selective amplification of a specific region. Quantitative PCR methods allow the estimation of the amount of this given sequence present in a sample[67]. Work flow of this process is visualized in Figure 7.

Figure 7. Schematic work flow of q-PCR method

Step 1: Isolate RNA

Based on their protocol of ADBC for RNA isolation, total RNA can be isolated from both fibroblasts cultured in non-stress conditions using Trizol (Invitrogen). Hereafter, chloroform will be added and incubated for 3 min at room temperature. The samples are mixed vigorously and then centrifuged. Centrifugation separate the biphasic mixtures into the lower red, phenol-chloroform phase and the upper colorless, aqueous phase. The RNA is then precipitated from the aqueous phase by mixing with isopropanol. After centrifugation, the supernate can be removed. Isolated RNA will be quantified by spectrophotometry and its integrity can be checked by electrophoresis on a 1% agarose/TBE gel containing ethidium bromide.

Step 2: Design and optimize primers

The process of DNA replication can't be initiated with out a primer. A primer is a small piece of DNA or RNA that is used as a starting point for the polymerase chain reaction (PCR). At this point DNA polymerases use the base upon which to attach new DNA nucleotides[67].

Primers are designed to span an exon-exon junction: cDNA does not contain any introns. Choosing the right primers is one of the most crucial factors determining the outcome and quality of the PCR, and using the wrong primer can even cause the reaction to fail. To choose the best primers for the task, pubmed can be used be entering the specific gene. If primers cannot be designed to separate exons, it is necessary to treat the RNA sample with RNase-free DNase in order to remove contaminating genomic DNA[67].

Two primers are always needed, one for the coding string and one for the template string. These are called the forward and the reverse primer[67]. For a-SMA primer mixtures can be found in table 2. To determine if the amplification product was exclusively from the RNA, a control without reverse transcriptase (RT) was occasionally included. The a-SMA RNA quality and amount of each specimen was controlled by analyzing the housekeeping genes B2M, GAPDH and YWHAZ.

Gene	**Accession number**		**Sequence 5'-3'**
a-SMA	NM_001613	Forward	CGTGTTGCCCCTGAAGAGCAT
		Reverse	ACCGCCTGGATAGCCACATACA
B2M	NM_213978	Forward	GGCATTCCTGAAGCTGAC
		Reverse	ATGTCGGATGGATGAAACC
GAPDH	NM_001256799	Forward	GAAGTATGACAACAGCCTCAAG
		Reverse	GTGGCAGTGATGGCATGG
YWHAZ	NM_145690	Forward	AGCAGAGAGCAAAGTCTTC
		Reverse	GCTTCTTGGTATGCTTGTTG

Table 2. a-SMA Primer sequences used for detection by qPCR[68].

Step 3-4: Reverse transcription and amplification of cDNA

According to their protocol of ADBC for cDNA synthesis RNA is first transcribed into complementary DNA (cDNA) by reverse transcriptase enzymes. cDNA is used as the template for qPCR reaction. Concentration of cDNA can be quantified by preparing a premix for each sample containing 5ul SSo SYBRgreen mix, 0.5ul 10uM primer mix, 2ul RNase-free H2O and 2.5ul cDNA.

Step 5-6: Run qPCR and analysis

qPCR can be performed using Sso Advanced qPCR-60degrees software and Bio-RAD CFX Manager. Data will be processed with the Bio-Rad Software. Statistical Analysis can be performed with Biogazelle.

3.1.3 Matrix functioning

To study the amount of contractility caused by mechanical stress, ECM stiffness can be measured. While gene-expression profiles provide a view of the inner workings of the cell, ECM stiffness gives us the most translatable outcome measure in the context of scar contracture[47,69].

3.1.3.1 Micro-indentation

Since the model consists of cells and ECM and this is viscoelastic material being an important feature of the mechanical behavior of ECMs[70], it is a difficult biomaterial to quantify mechanically. The most commonly used technique for micromechanical characterization of biological tissue is Atomic Force Microscopy. The technique makes use of a small radius tip to locally probe the mechanical response of a material to a compressive stress. Unfortunately, as demonstrated in a study of Antonovaite et al. (2018), during piezo-control tests, the indentation depth and speed differed despite of the same protocol, causing stiffness variations to occur[71].

A more suitable alternative is micro-indentation. Micro-indentation can be used to measure micromechanical properties of thin sections of the samples, while assuring constant indentation depth and constant indentation speed[69]. The technique allows the quantification of stiffness and load-displacements to provide storage and loss moduli. These are properties of viscoelastic materials and can be calculated from either free or forced tests in shear, compression or elongation. Information about these moduli is interesting since the substrate and thus attached samples will be enforced to deformation due to the mechanical stretch applied by the stretch device. Storage moduli represents the elastic portion of the stiffness while loss moduli represents the viscous portion[71,72].

To measure the mechanical properties of three-dimensional complex and irregular materials, like ECM, a tool is used that combines a cantilever-based micro-indentation setup with OCT imaging system: a cantilever introduces a small indentation at specific regions, while the OCT system is used to determine and visualize the deformation profile near the indentation site from the recorded motions[72]. Setup of the system is shown in figure 8.

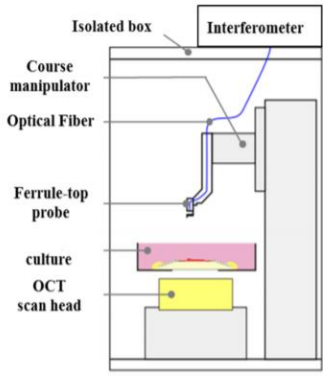

Figure 8. Schematic representation of the micro-indentation setup. The indentation arm comprises an XYZ micromanipulator, a piezoelectric transducer, a single mode optical fiber used to readout the bending of cantilever and a ferrule-top cantilever indentation probe connected to an interferometer. The sample can be visualized by OCT from below, while the mechanical measurements are performed by indentations from above. Reproduced from Marrase M. et al. (2019)[72].

3.2 Formulating a suitable stress protocol

The first sub goal was to formulate a suitable mechanical stress protocol that mimics burn splinting techniques. Parameters that influence mechanical stress will be set, which are type of stress, dimension and technique, but also magnitude of strain, frequency and duration. Type of stress can vary between compression, tension, shear, bending, torsion or alternative forces. Different types of mechanical stress are described in literature: compression, tension, shear, bending, torsion, alternative forces. In our model we chose to apply tension or 'stretch' as mechanical stress, as this is the form of deformation most accurately resembles deformation in the clinical situation (i.e. splinting). Assumptions were made on multiaxial skin deformation in reaction to stretch. This clinical multiaxial reaction is in three dimensions which is in compliance to the experiment since the model consists of fibroblasts and a three-dimensional ECM and not with a single monolayer.

Stretch dimension describes the axial range of the dimension of cell resulting from applied stress, for example uniaxial and biaxial dimensions. As the terms predict, uniaxial stretch provides stretch on one axis, while biaxial stretch provides stretch uniformly in two axial directions[35].
Techniques for a suitable stretch protocol refer to dynamic, static and combined protocols. Dynamic stress is a series of mechanical loads that are executed repeatedly, while static stretch entails a singular motion held in place for a certain period.
Strain is the change in deformation relative to elongation or surface of a material. Frequency and duration refer to the number of times stretch is applied in a selected time scale.

An evidence-based stress protocol was identified. On the one hand, a literature review was started in which mechanical stretch was applied to human dermal fibroblast and derived ECM constituents in normal skin, burnt skin and pathological scars. With help of this literature study, previously applied stress stretch protocols were compared.
On the other hand, a clinically based protocol was formulated on the basis of interviews with a physiotherapist working in the field of burns care and splinting.

The strength of the experimental evidence (literature research) and a more empirical protocol were considered and selected parameters were set.

3.3 System selection

The second sub goal was to select a system that enables mechanical stretching of extensible substrates that facilitate the growth of fibroblasts and their derived ECM. To reach this goal, the device to select needed to adhere to certain requirements:

(1) the device must provide application of selected mechanical stress protocol to the cell cultures. Therefore, (2) the device must be programmable for the selected stress protocol and (3) the installed stress to the device must be transferrable from the device to the cells, which can be fulfilled by using

flexible substrates where the cells are attached and growing on. For this reason, (4) these flexible substrates must be compatible with the device.
Next to the tensional aspects, (5) the system needs to provide a culture environment where fibroblasts can successfully grow and remodel ECM in response to the changing physiological environment. Therefore, the material of the substrate of the culture dish where the cells are growing on should meet requirements like: (a) The substrate material should be extensible, and compatible with the chosen stretching device, (b) must be nontoxic and should enable adhesion and cell proliferation, (c) should permit observations of the cells by microscopy technique, (d) and the substrate should function as a culture dish in which a sufficient volume of culturing medium can be placed without overflowing, even when during application of the stretch protocol.
Furthermore, for culture conditions, (6) the device must be easy to sterilize and (7) practical in daily use for culture medium replacement. In addition, (8) the system set up must be compatible with the selected measurements techniques. Therefore, (9) the device must be transparent to facilitate microscopy techniques and periodic visual inspection of the samples as microbial contamination is likely in this context.
Lastly, (10) costs must be taken into account in device selection.

A system that fulfilled most of the requirements and was provided by ADBC, was the MechanoCulture B1 (MCB1) stretching apparatus (CellScale® Univert Biomaterial Tester, UK). This stretching device consists of four main parts (Figure 9): (1); a radial snowflake attached with 24-pin mounting ring; (2) on this 24-pin scaffolds, tissues but also flexible substrates with cell cultures onto it can be puncture-mounted and stretched according to the specified protocol (requirement 3,4) (3); a deformable component used to generate radial motions from a linear input. A secondary component is used to transfer 8 points of motion into the 24 pins. This multitude of attachment points distributes the load so that individual attachment points will not tear the substrate, (4); and a motor driven by a computer controlled interface program of Univert. Compression. Biaxial stretch up to 20%, frequency, displacement velocity, duration, and parameters such as load technique and strain can be specified in the software application and programmed to run stretch patterns (requirement 1,2).

Since the device is closed from the outside environment by a removable cover, the device is practical to use for daily medium refreshments. Furthermore, sterilization of the device is straightforward.

Some limitations remained. First, the MCB1 does not come with expendable substrates that can function as a culture dish. Moreover, non of the MCB1 parts are transparent and so the system is not compatible with selected microscopic measurements. The design of the test chamber had to be modified in order to make it compatible with routine microscopic analysis, periodic visual inspection, and OCT imaging during micro-indentation.

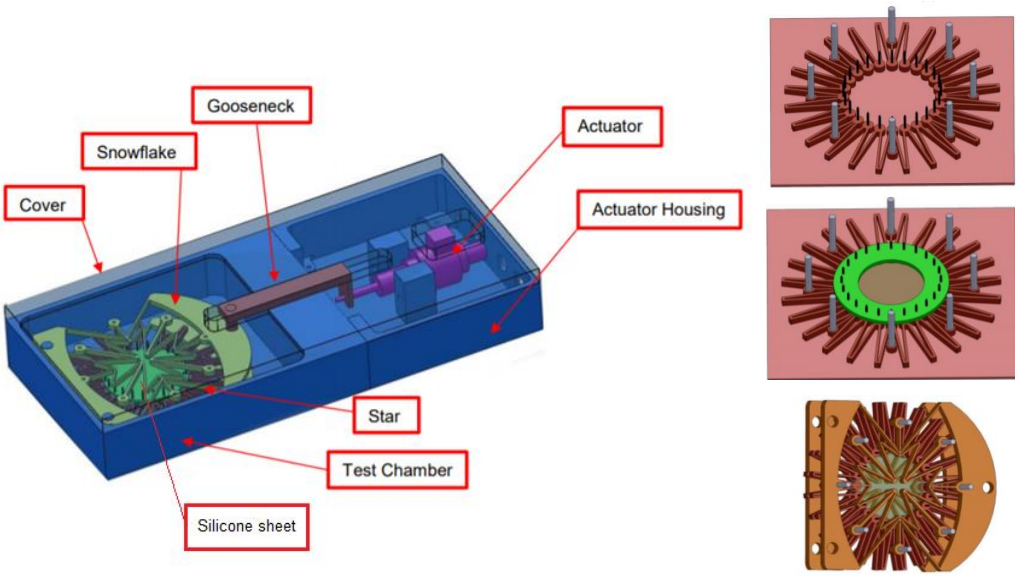

Figure 9. Overview MCB1 parts. Reproduced from User Manual © 2017 CellScale

Earlier mentioned literature study was conducted to compare substrate materials in currently used stretch devices for the application of stretch to culturing fibroblast. With help of this study, minor technical adaptations were made to MCB1.

3.4 Culture conditions and optimization

The third sub goal was to create and optimize conditions in which fibroblasts can be successfully cultured on an extensible substrate. Conditions are chosen to mimic physiological conditions, while also optimizing growth. Growth can be characterized by cell division (mitosis) or by other processes, such as differentiation, during which cells can change morphological and phenotypical characteristics.

Culturing cells is characterized by the following workflow: obtaining skin samples from surgical waste, cell isolation, cell cultivation and cell proliferation, see figure 10.

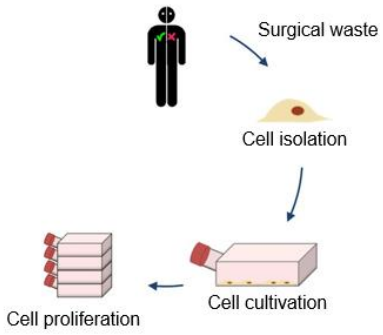

Figure 10. Workflow for culturing cells

Skin samples

Skin samples were obtained from the burn center of the Red Cross Hospital Beverwijk, Netherlands. Excised skin was used as this was designated surgical waste material after routine excision; national guidelines stipulate that patients provide oral consent to the use of surgical waste, which was obtained preoperatively. Healthy skin samples were obtained after cosmetic abdominoplasty surgery, eschar tissue was obtained after excision of deep partial thickness or full thickness burns. Tissue was immediately wrapped in damp gauze and stored at 3°C.

Fibroblast isolation

Skin samples were cut into manageable size. Dermis and epidermis were separated enzymatically by incubating skin samples in a saline solution with 0.25% dispase II (Boehringer Mannheim, Germany) at 37°C for 1 h. Dermal and eschar tissues were washed, weighed, and minced with sterile scissors. Samples were then incubated for 1.5—3 h in 2 ml of saline containing 0.25% dispase II/collagenase A (Boehringer, Mannheim, Germany) for every gram of tissue at 37°C under continuous agitation.

Cell cultivation

After isolation, fibroblasts were cultured in culture flasks under carefully controlled conditions. In this so-called adherent culture, cells grow in a monolayer on a substrate. Standard substrate for cell culturing, flasks and petri dishes are made of high-quality polystyrene material and are pre-sterilized by gamma irradiation[73]. However, in our model, flexible substrates are used. When other materials are used as culture substrate, it's surface is coated and treated prior to cell culturing to facilitate cell attachment and growth. Chapter 3.4.1 describes the strategy of optimal coating selection whereas chapter 3.4.2 for optimal surface treatment. Based on these selections, characterization of substrate was conducted in chapter 3.4.3.

Fibroblasts cultures were maintained under appropriate temperature and gas mixture of typically 37 °C, 5% CO2 and in culture medium. This medium is essential for cell growth and composed of different nutrients (like amino acids, vitamins, minerals, growth factors), varying for each cell type[74]. Chapter 3.4.4 describes the strategy of optimal culturing media selection.

Cell proliferation

When the monolayer of cells covers over 80% of the surface of the culture flask, the layer is deemed to be confluent. At a higher level of cell density, contact inhibition will cause the cells to lose their proliferative activity and ECM formation and they will commence differentiation[75]. To prevent this, cells are sub cultured in a lower concentration in new flask. This 'passing of cells' will maintain the proliferative rate of the cells, making sure that an adequate number of cells is reached for the final experiment[76].

3.4.1 Coating selection

Coating regimes are commonly used to reduce for example hydrophobicity of substrates, making the surface more appropriate for cell cultures: coating the surface will make sure that surface is correctly charged, allowing cells to attach and spread via integrins and other cell surface receptors[77–79].

The selection of coating regimes used for comparative experiment 1 was based on literature in which different coatings, for example collagen type I[40–42,50–52] and gelatin-, were used for the attachment of fibroblasts. When collagen is used as coating, successful adaptation is facilitated in terms of expression of cell-specific morphology and function, resulting in greater attachment[77]. Gelatin is a biodegradable derivative of collagen, and therefore gelatin can be coated on substrates to obtain desired cell adhesion[80]. Since these studies show well cell growth, adhesion and proliferation on substrates, collagen type I and gelatin coating were selected for a direct comparison, see **experiment 1**.

Experiment 1: Coating selection

Two coating conditions were compared on their effect on the production of collagen matrices by cultured fibroblasts: (1) Gelatin-A coating; (2) Collagen I coating.

Gelatin coating (Gelatin-A from porcine skin, Sigma) was applied according to the manufacturer's protocol by dissolving 2% gelatin powder in PBS.

Collagen type I coating (Rat tail, Sigma) was applied according to the manufacturer's protocol, by dissolving collagen to 50 µg/mL in 0.02 M acetic acid at the final.

After sterilization, the solutions were applied to the substrate surface and incubated for one hour at 37°C with 5% CO2. Hereafter, HEF and HDF were harvested and seeded on these substrates, and cultured in supplemented Dulbecco's Modified Eagle's Medium (DMEM) with 10% FCS, 1% L-glutamine, 1% streptomycin/penicillin (Gibco, Pastley UK).

Condition	*Fibroblast type*	*Sample size*
Gelatin-A coating	HEF donor 1	2
	HDF donor 1	2
Collagen-I coating	HEF donor 1	2
	HDF donor 1	2

Selection was based on the general density of the produced ECM using SHG microscopy on only one sample. Combined 2PEF/SHG images were acquired and based on z-stack counting (2um per image slice) collagen matrix thickness was determined at ultimate day of culturing.

3.4.2 Substrate surface optimization

An additional method to the coating regimes is crosslinking or plasma treatment. Crosslinking has been used in coating methods on biomaterials because it results in a dramatic increase in the stiffness of the coatings and also tends to smoothen these coating surfaces, supporting cell activity[81,82]. Glutaraldehyde and ethanolamine are commonly referenced cross-linkers with this type of functionality[83]. When proteins or peptides that naturally contain at least one primary amine group are brought in contact with the cross-linker, they will covalently bind with the cross-linker and attach to each other. Currently, the chemistry

of these coupling reactions is well understood and it has been proven to create adherent surfaces for various cell types[83].

Plasma treatment is a an attractive option creating free radicals by cold gas plasmas, since it has four major effects: surface cleaning, ablation, crosslinking, and surface activation, resulting in higher adhesion of cells to hydrophobic substrates[84].

Crosslinking and plasma modification techniques were investigated in comparative **experiment 2**. Coating was applied based on best outcomes in experiment 1.

Experiment 2: Prior surface modification and cross-linked coating of substrates

In this experiment we compared 4 coatings and surface modifications for their effect on collagen matrices produced by cultured fibroblasts: (1) gelatin-A; (2) gelatin-A crosslinked; (3) plasma surface modification (plasma); (3) crosslinked gelatin-A with prior plasma surface modification (plasma gelatin-A crosslinked).

The gelatin coating procedure was described in experiment 1.
Crosslinking gelatin was done by washing the gelatin-coated samples with DPBS, and subsequently treating them with 1% glutaraldehyde solution for 30 minutes at room temperature. After washing again with DPBS, sheets were incubated with 1M ethanolamine for 30 minutes at room temperature.

Plasma surface modification was performed with a plasma technology device (TUeindhoven, pulser).

HEF from two donors were seeded on these substrates and cultured in supplemented Dulbecco's Modified Eagle's Medium (DMEM) with 10% FCS, 1% L-glutamine, 1% streptomycin/penicillin (Gibco, Pastley UK).

Condition	***Fibroblast type***	***Sample size***
Gelatin-A	HEF donor 1	2
	HEF donor 2	2
Gelatin-A crosslinked	HEF donor 1	2
	HEF donor 2	2
Plasma	HEF donor 1	2
	HEF donor 2	2
Plasma gelatin-A crosslinked	HEF donor 1	2
	HEF donor 2	2

The best coating was selected based on the general density of the collagen matrices produced by the cultured fibroblasts, as determined with SHG microscopy on only one sample. Combined 2PEF/SHG images were acquired and based on z-stack counting (2um per image slice) collagen matrix thickness was determined at day 4 and ultimate day of culturing.

3.4.3 Substrate characterization

Substrate effects cell adhesion and proliferation. Therefore, it is useful to do measurements on the characteristics of the selected substrate in terms of strain distribution and stiffness.

The in-plane strain of the membrane is important, as the cells attached on the silicone sheet are expected to experience the same deformation as the silicone sheet itself. However, the stretch set in the device can deviate from the stretch that is actually performed on the cells. Therefore a strain analysis was conducted. Methods are described in **experiment 3.**

Furthermore, since stiffness of the substrate can effect cell adhesion[85], it would be valuable to also do measurements on the ultimate substrate with optimal surface in non stretched and stretched conditions. In a study of Sun et al. (2018)[85], cells became more spread and more adhesive on substrates of higher stiffness. This is due the cells 'sense' stress in their environment. Focal adhesions provide the pathway of force transmission from inside the cell to the elastic matrix. Due to mechano-transducer signals the cell is able to create a force to deform matrix[86]. These stiffness-specific characteristics of cells can influence future outcomes when using this burn splinting model, in terms of cell organization.

The effect of cross-linked coating and stretch on stiffness of the substrate was done by a comparative **experiment 4** by conducting optimized substrate surface regimes resulting from experiment 1 and 2, and measuring its effect on substrate elasticity by using micro-indentation techniques.

Experiment 3: Strain analysis of substrate surface

In this experiment we performed a strain analysis with help of particle image velocimetry (PIV) analysis to determine the distribution of the stretch that we apply to the silicone sheet. This was determined by tracking the displacement of random dot markers on silicone rubber surfaces and stretching the flexible bottom membranes with levels that corresponded to 0 and 20% strain (see figure E3). At these levels, images were acquired using a 4.7-inch Iphone 7 camera with a resolution of 1,334 x 750 pixels (326 ppi) at the chosen field of view at one day of stretching. Two analyses were done in which centralization of the images was applied or not. ImageJ PIV plugin program was used to apply PIV automatically and determine the strain distribution based on the two obtained photos (relaxation, strain 20%). This program was achieved from https://sites.google.com/site/qingzongtseng/piv.

(a) 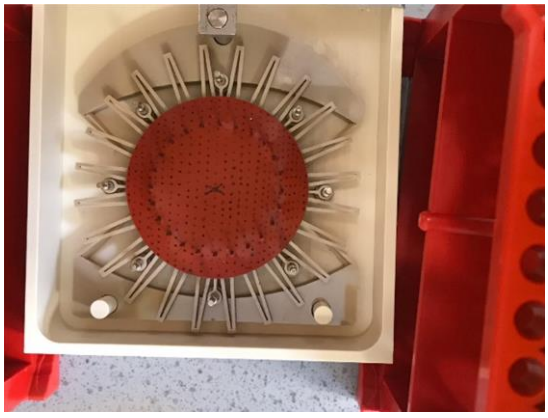 (b) 

Figure E3. Dot markers on silicone rubber surfaces in (a) relaxation (0%) and (b) stretch (20%) level. Stretch direction is visualized by the blue arrow.

Experiment 4: Effect of optimized substrate surface and stretch on stiffness of the substrate

In this experiment we compared 3 conditions on the effect of substrate elasticity: (1) non-coated in unstretched state; (2) non-coated in stretched state and (3) coated in unstretched state. Each dataset consists of 10 measurements.

We analyzed the effect of coating and stretch on substrate in terms of stiffness by using micro-indentation techniques. To compare stiffness distribution on the substrate we measured stiffness in the middle and at the edge of the substrate for non-coated silicon substrates in stretched state. Analysis of the results was done in MATLAB. Significance was tested with help of student's t-test in MATLAB.

3.4.4 Culture medium optimization

The choice of media not only influences cell proliferation, it is of utmost importance in the timely production of ECM[74]. Reducing the time fibroblast need to produce an ECM, reduces the risk of premature contracture or contamination. Recipes for growth media can vary in pH, glucose concentration, growth factors, and the presence of other nutrients. The growth factors used to supplement media are often derived from the serum of animal blood, such as fetal bovine serum (FBS)[74]. Optimization of medium content can reduce the time needed to provide an experimentally relevant fibroblast derived matrix[74].

Fibroblast growth medium used at ADBC consists of Dulbecco's Modified Eagle Medium (DMEM) supplemented with 10% FCS, 1% penicillin/streptomycin and 1% glutamin. Supplementing growth factors and nutrients can expedite the formation of ECM significantly[87]. Ascorbate is an essential requirement in normal connective tissue metabolism and for collagen formation, and stimulates the production of collagen[88]. Therefore, we decided to add l-ascorbic. An experiment was performed to determine the appropriate concentration of l-ascorbic acid added to the growth medium of the cell cultures. See **experiment 5.**

To reduce culture time, different medium formulas were tested in a comparative experiment 5. Therefore, we selected three different medium contents: (1) Fibroblast growth medium used at ADBC consisting of Dulbecco's Modified Eagle Medium (DMEM) supplemented with 10% FCS, 1% penicillin/streptomycin and 1% glutamin (2) a commercial mixture marketed specifically for collagen matrix production (CNT-05), and (3) a different commercial product from the same manufacturer that is marketed as a more efficient growth medium (CnT-PR-ECM). See **experiment 6**.

Experiment 5: Magnitude of l-ascorbic acid stimulation

We compared three different concentrations of l-ascorbic acid stimulations to the cell cultures: (1) 50 ug/ml l-ascorbic acid (2) 65 ug/ml l-ascorbic acid and (3) 75 ug/ml l-ascorbic acid.

HEF and HDF from one donor were seeded on standard culture dishes and cultured in supplemented Dulbecco's Modified Eagle's Medium (DMEM) with 10% FCS, 1% L-glutamine, 1% streptomycin/penicillin (Gibco, Pastley UK). Half of the supplemented culture medium was refreshed daily supplemented with the above mentioned concentrations of vitamin C .

Condition	***Fibroblast type***	***Sample size***
50 ug/ml	HEF donor 1	2
	HDF donor 2	2
65 ug/ml	HEF donor 1	2
	HDF donor 2	2
75 ug/ml	HEF donor 1	2
	HDF donor 2	2

The optimal concentration was selected based on the general density of the collagen matrices produced by the cultured fibroblasts, as determined with SHG microscopy on only one sample. Combined 2PEF/SHG images were acquired and based on z-stack counting (2um per image slice) collagen matrix thickness was determined at ultimate day of culturing.

Experiment 6: Growth medium content selection

In order to optimize cell growth medium content, we compared three different supplemented media used for fibroblast cultures: (1) supplemented Dulbecco's Modified Eagle's Medium (DMEM) with 10% FCS, 1% L-glutamine, 1% streptoycin/penicillin (Gibco, Pastley UK) (supp DMEM). (2) CellnTech medium (CNT-05); and (3) CellnTech (CnT-PR-ECM);

HEF and HDF from one donor were seeded on standard culture dishes and cultured in supplemented Dulbecco's Modified Eagle's Medium (DMEM) with 10% FCS, 1% L-glutamine, 1% streptomycin/penicillin (Gibco, Pastley UK). Half of the supplemented culture medium was refreshed daily supplemented with the earlier selected concentrations of vitamin C determined in experiment 4.

Condition	***Fibroblast type***	***Sample size***
Supp DMEM	HEF donor 1	2
	HDF donor 2	2
CNT-05	HEF donor 1	2
	HDF donor 2	2
CnT-PR-ECM	HEF donor 1	2
	HDF donor 2	2

The best growth medium was selected based on the general density of the collagen matrices produced by the cultured fibroblasts, as determined with SHG microscopy on only one sample. Combined 2PEF/SHG images were acquired and based on z-stack counting (2um per image slice) collagen matrix thickness was determined at ultimate day of culturing.

3.5 Validation of the attained in vitro burn splinting model

In this part of the study the ultimate designed model with extracted parameters from the previous experiments was tested on the feasibility of the model. Methods for formulated stress protocol, selected system and optimized culture conditions were examined according to the final protocol, which can be found in Appendix 2. Selected outcome measures in this study were matrix organization and fibroblast functioning. Matrix organization measurements were taken on one single sample in non-stretched, static stretched an dynamic stretched culture conditions, on the ultimate day of the stretch regime. Therefore, number of relevant z-stacks were counted and these were analyzed for matrix synthesis, density and collagen fiber alignment. Fibroblast functioning measurements were taken on non-stretched samples cultured in standard culture dishes (standard non-stretch) at day 1 and ultimate day of the experiment.

HEF and HDF stored in 2014 were obtained from one donor. In the experiment we also include HDF as a baseline to compare with the HEF group. In this way we enable comparison of a healthy condition with a pathological condition. Statistical significance of matrix organization results were calculated with help of student's t-test. Experimental conditions are shown in table 3.

Condition	***Fibroblast type***	***Sample size***
Standard non-stretch	HEF (donor 1)	2
	HDF (donor 1)	2
Non-stretch	HEF (donor 1)	2
	HDF (donor 1)	2
Static stretch	HEF (donor 1)	1
	HDF (donor 1)	1
Dynamic stretch	HEF (donor 1)	1
	HDF (donor 1)	1

Table 3. Characteristics of experimental conditions defined in validation of the designed in vitro burn splinting model.

4. Results

A summarized overview of the results is shown in figure 11. The following chapters will clarify these results.

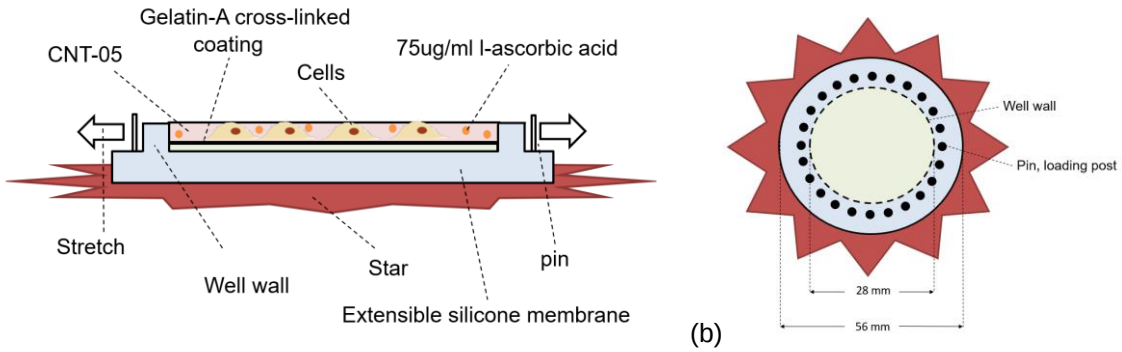

Figure 11. Schematic of the method of stretching the fibroblast-populated extensible silicone substrates. Stretch is applied to the edges of the substrate with help of the 24 pins, resulting in controlled biaxial stretch in (b) top view of the circular well showing dimensions of the well and loading post.

4.1 Formulating a suitable stress protocol

Stretch dimensions were categorized into uniaxial (n=15) or biaxial direction (n=5) (Table 4). Since in reaction to stretch skin tension lines show deformation in different axes, stretching of the skin is inherent to more than one dimension. Therefore, the initial approach utilizes biaxial stretch over uniaxial stretch.

Techniques for mechanical stress were categorized into stretching dynamically or statically, see table 4. The vast majority of the included articles used dynamic stretching as the experimental arm, with static stretching as control groups. Only two studies applied static stretch as an experimental intervention. Since both dynamic and passive splinting regimes are used clinically, they were both deemed relevant. Therefore, the initial approach utilizes both dynamic and static stretch.

As can be seen in table 4, stretch varied from two to twenty percent deformation, with a frequency ranging from 0.5 to one Hertz. The duration of intervention ranged from one to twenty-four hours to 6 days or more. However, motivations for these parameters settings were often not specified, or were general approximations of strain during locomotion. Stretch frequencies similar to respiratory or cardiac rates were also provided as a rational (Table 5).

	Fibroblast type	Stretch device	Substrate	Stretch dimension	Technique	Strain (%)	Frequency (Hz)	Duration
Balestrini (2006)[36]	Dermal	FX-4000 †		Biaxial	Dynamic	16	0.2	8d
Du (2013)[48]	HS	FX-4000 †	PDMS	Uniaxial	Dynamic	10	0.17	0,6,12h
Huang (2013) [49]	Dermal	STB-140 *	PDMS	Uniaxial	Dynamic	20	0.17	24h
Ishise (2015)[50]	Dermal, HS	STB-140 *	PDMS	Uniaxial	Dynamic	20	0.17	24h
Jiang (2016)[51]	Dermal	Custom built	PDMS	Uniaxial	Dynamic	20	1	1-6d
Kessler (2001)[52]	Dermal	FX-3000 †	PDMS	Biaxial	Dynamic	20	1	4,12,20,24h
Kim (2013)[53]	Dermal	Custom built	PDMS	Uniaxial	Dynamic	10	0.5	1h
Kuang (2015)[54]	Dermal	Custom built	PDMS	Uniaxial	Dynamic	10	0.1	24, 36, 48h
Kuang (2016)[55]	Dermal, HS	FX-4000 †	PDMS	Uniaxial	Dynamic	10-20	0.1	24h
Neidlinger-Wilke (2002)[38]	Dermal	Custom built	PDMS	Uniaxial	Dynamic	8	1	0.5, 1-6, 8, 10, 12, 14, 16, 24h
Nishimura (2007)[39]	Dermal	FX-4000 †	PDMS	Biaxial	Dynamic, Static	10	0.17 - 0.1	1-7d
Reichenbach (2014)[40]	Dermal	FX-4000 †	PDMS	Uniaxial	Dynamic	16	0.5	5, 24h
Binda (2014)[41]	Dermal	FX-4000 †	PDMS	Uniaxial	Dynamic	10	1	0, 6, 12, 24, 48, 72, 96h
Shikano (2015)[42]	Dermal	Custom built	PDMS	Uniaxial	Dynamic	2-2,5	1	4d
Syedain (2011)[43]	Dermal	Custom built	PDMS	Uniaxial	Dynamic	5-15	0.5	2,5, 7w
Tokuyama (2015)[44]	Dermal, HSE	STB-140 *	Latex	Uniaxial	Dynamic	10	1	5d
Wang (2000)[45]	Dermal	Custom built	PDMS	Uniaxial	Dynamic	4,8,12	1	24h
Wang (2006)[46]	Dermal, KS	Custom built	PDMS	Biaxial	Static	10	n/a	0,3,6,24h
Weidenhamer (2013)[47]	Dermal	Custom built	PDMS	Biaxial	Dynamic	5	0.5	3w
Zhang (2014)[19]	Dermal	STB-140 *	PDMS	Uniaxial	Dynamic	10	1	8h

Table 4. Overview of results of literature study. Characteristics of stretch devices and their parameters in studies where stretch is applied to HDF. HS = hypertrophic scars, KS = keloid scars.

Balestrini (2006)[36]	Not specified
Du (2013)[48]	Not specified
Huang (2013) [49]	Not specified
Ishise (2015)[50]	Not specified
Jiang (2016)[51]	Respiratory rate, heart rate, previous study on myoblasts (*Soltow 2010* [89])
Kessler (2001)[52]	Not specified
Kim (2013)[53]	Approximate strain during locomotion
Kuang (2015)[54]	Not specified
Kuang (2016)[55]	Previous studies which lacked discriminating stretching strategies (*Kim 2013*[53]), previous study on tenocytes (*Arnoczky 2002*[90])
Neidlinger-Wilke (2002)[38]	Previous study on osteoblasts
Nishimura (2007)[39]	Not specified
Reichenbach (2014)[40]	Not specified
Binda (2014)[41]	Not specified
Shikano (2015)[42]	Heart rate, approximate human skin elongation in daily activities
Syedain (2011)[43]	Not specified
Tokuyama (2015)[44]	Heart rate
Wang (2000)[45]	Previous study on osteoblasts
Wang (2006)[46]	Previous study which lacked discriminating stretching strategies (*Lindahl 2002*[91])
Weidenhamer (2013)[47]	Not specified
Zhang (2014)[19]	Not specified

Table 5. Provided motivations for chosen stretch strategies in included articles.

Current status of literature result in no properly informed settings for these parameters. In consultation with physiotherapists who deal with splinting on a daily basis, a clinically relevant protocol was examined. Given the level of evidence in literature, an empirical protocol was chosen. This resulted in either static deformation of 20% (relative to original surface) every 24 hours or dynamic deformation of 1Hz, 20% for 2 hours followed by a static stretch of 20% for 10 hours. Duration time was set based on cultivation duration in experiment 1-5, which resulted in 9 till 10 days.

4.2 System selection

As can be seen in table 4, earlier studies frequently utilized the STREX Cell Stretching System (STB-140) for uniaxial stretch. The Flexcell Stress Systems (FX-4000, FX-3000) were used for both uniaxial and biaxial stretch. These devices function by means of vacuum application to the undersurface of a substrate-like substrate. Next to these, custom-built stretching devices were designed for both uniaxial and biaxial stretching directions, using flexible bottom polydimethylsiloxane (PDMS) or latex chambers. In all these devices parameters as strain, frequency and duration of stretch can be set manually.
Devices used for biaxial stretch were applicable to our model. However, high costs, incompatibility with the chosen analysis techniques, and non-adjustable substrates meant this device was not applicable to the desired model.

4.2.1. Device modifications

The choice for an extensible substrate was based predominantly on the above-mentioned literature review. The vast majority of studies (Table 4) used PDMS as an extensible substrate, showing that PDMS is capable of sustaining growth of dermal fibroblasts. PDMS is a variably flexible polymer, and its affordability and availability in many forms make it a popular choice for this type of research. Characteristics of PDMS, such as gas permeability, optical transparency, and flexibility make the material appealing for cell culture devices. In addition, it is generally regarded as inert, non-toxic and fully bio-compatible. Based on the literature review and PDMS properties, we suggest that PDMS substrate fulfill to all requirements. Sylgard184 (Sylgard 184, Dow Corning, USA) was the chosen PDMS type, as it is commonly used for fabrication of cell culture devices and is available in a transparent version which ensures compatibility to microscopic techniques[78] . This PDMS solution can be prepared using a standard protocol. First, a silicon elastomer prepolymer (base) and a cross-linker (curing agent) are thoroughly combined at chosen mixing ratio. Next, the mixture is placed in a vacuum for 20 min to remove air bubbles trapped in the uncured liquid silicon. Finally, the mixture is cured in an oven (VentiCell™ Drying Ovens, Fisher Scientific) at 65◦C for 4h[18].

Lee et al. (2004)[92] showed that the formulation of mixing ratio and surface treatment are optimized for each cell line, indicating mixing ratios of 10:1 for fibroblasts. However, in a trial for this mixing ratio, we found that we needed higher flexibility of the silicone substrate. For this reason we chose to use a mixing ratio of 15:1.

Sufficient curing times will ensure the complete curing of PDMS, leaving no un-crosslinked polymers within the material that can potentially contaminate the culture medium.

To make the substrate function as a culture dish, where a sufficient volume should be present for culture medium also when applying the mechanical stress, a mold design was designed where in the PDMS solution was cured, for an easier production of substrates. This resulted in a flat disk with a 3 mm circular ridge in the middle. The area within this circle was to be the culturing area which holds a minimum of 4ml of culture medium, with a ridge to keep the medium from flowing out. Based on the determined dimensions, a CAD-drawing was designed with help of SolidWorks, and manufactured with (1) three-dimensional printing techniques using polylactic acid (PLA) (Ultimaker 2+, 0.4mm nozzle) or (2) sanding a solid block of polyvinylchloride (PVC). Furthermore, a 1 mm thick glass cover slip with a diameter of 28 mm was glued onto the platform in the middle of the mold to create a flat foundation for the eventual seeding of cells (Figure 12a-c).

Immediately noticeable from figure 12d-e was that the manufactured silicone substrates yielded good results when they were cured in the PVC molds. These cured silicone substrates did not stick to the surface and cracks were prevented, on contrary to the PLA molds. Curing time of 4 hours seemed to give good results based on the substrates to be flexible, did not tear when pulled and were not sticky or wet.

The cover and the chamber were re-manufactured by means of a transparent (retractable) polymethyl methacrylate (PMMA). Design was made in Solidworks. see figure 13 and 14. Dimensions of the original test chamber and case were measured and used for this design. Dimensions of original elements and manufactured transparent elements were similar. Bottom of test chamber was retractable. Therefore, new manufactured elements were useful for implementation to the MCB1.

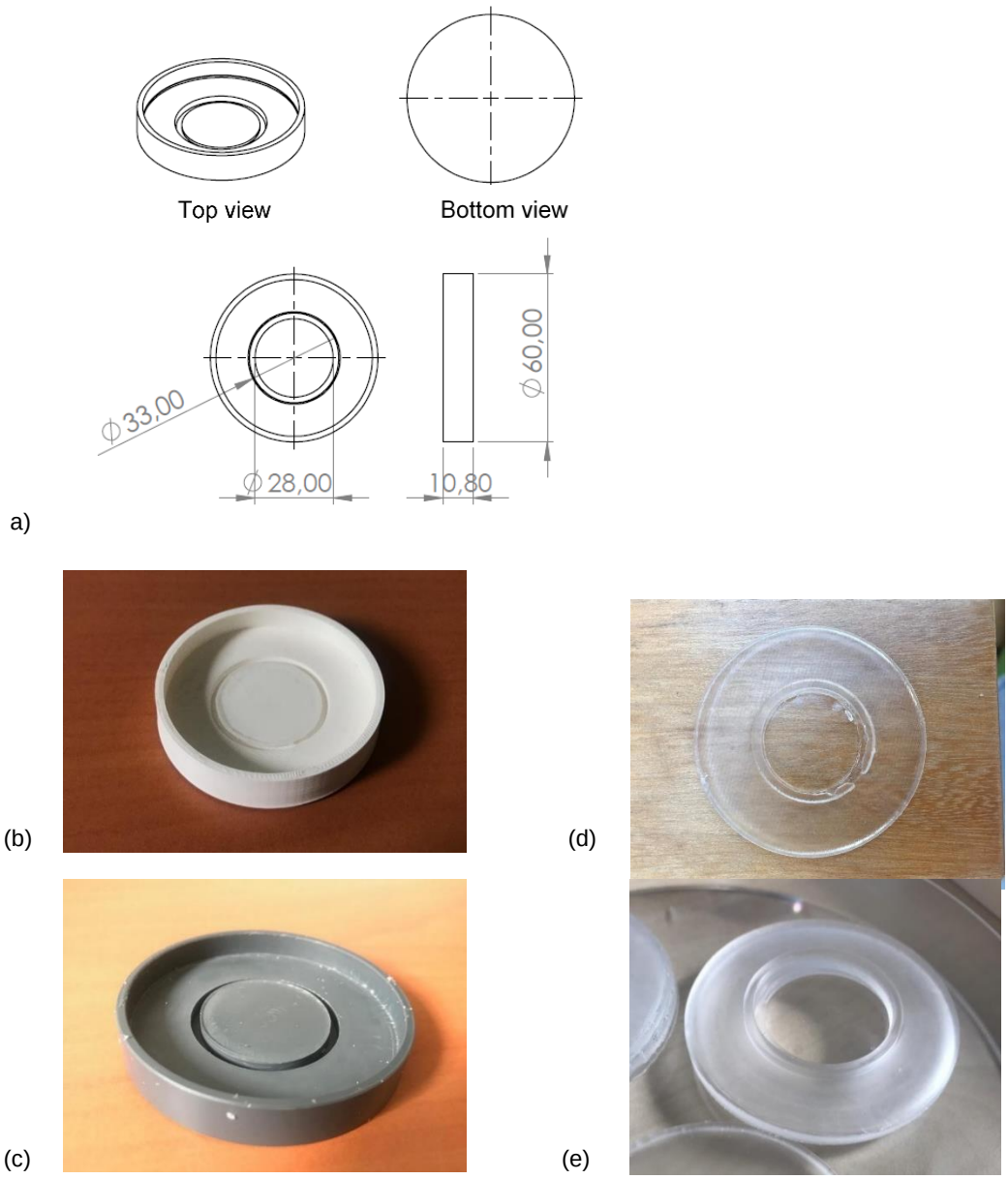

Figure 12. (a) CAD Design of the mold with 3mm height platform in the middle. On the platform in the middle a circular perspex sheet was fixed with diameter of 28mm and thickness of 1mm. (b) Manufactured design of the mold by three-dimensional printing technique (PLA material) with 3mm height platform in the middle. On the platform in the middle a circular perspex sheet was fixed with diameter of 28mm and thickness of 1mm (c) with sander machine (PVC material) (d) manufactured silicone substrate in PLA mold and (e) in PVC mold.

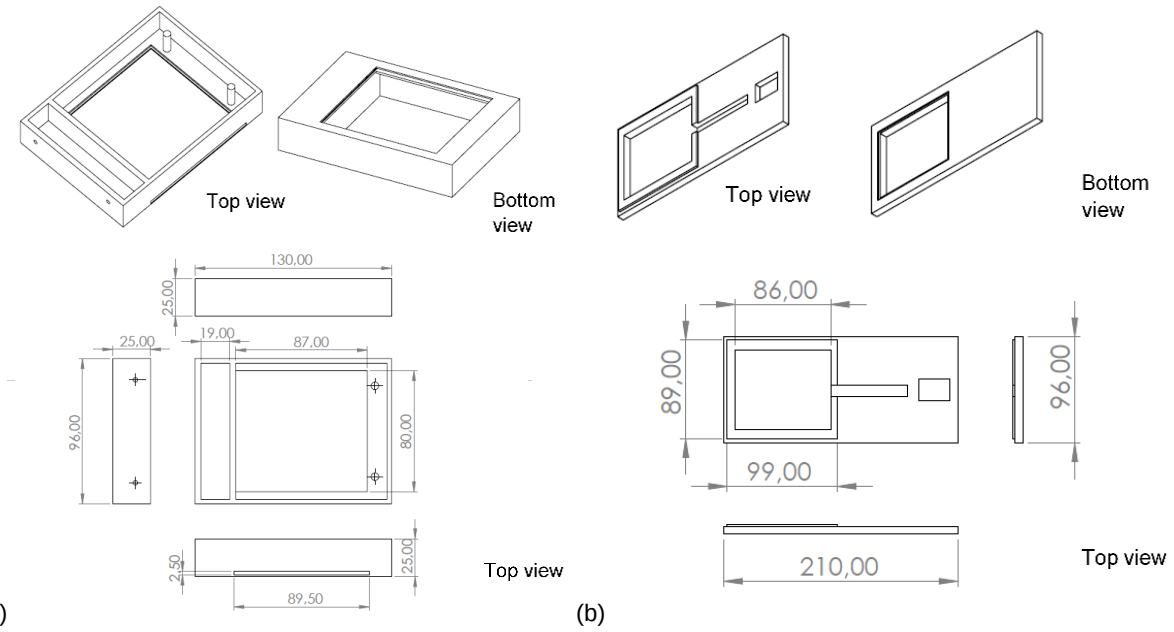

Figure 13. CAD design of the (a) test chamber and (cover). Dimensions are in mm. In the bottom of the test chamber a slide of 1.25x2.5mm is made in which the perspex sheet of 82,5x89,2mm can be attached or retracted. In the gap of the cover a perspex of 99x89mm sheet can be attached.

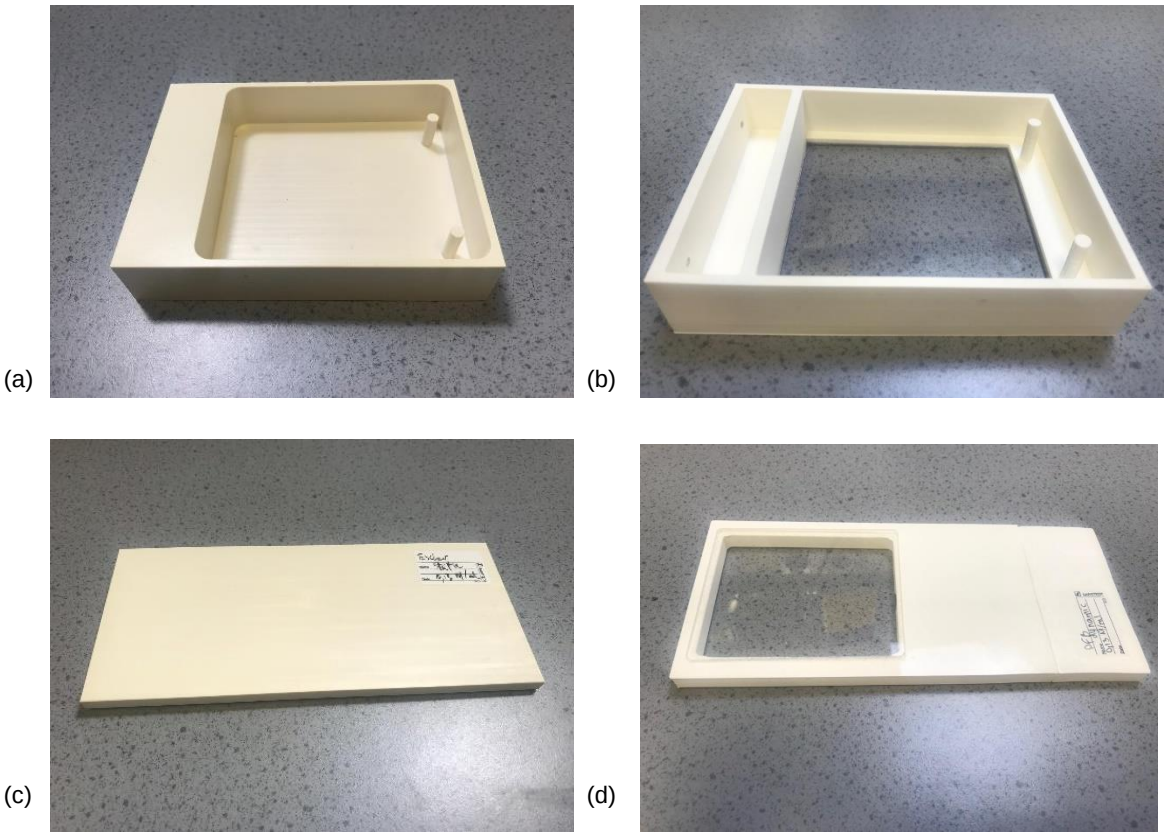

Figure 14. (a) original test chamber; (b) manufactured test chamber; (b) original cover; (c) manufactured cover.

4.3. Culture conditions and optimization

4.3.1 Substrate surface optimization

Sufficient ECM was produced by the fibroblasts after 21 days of culturing. The results of the two experiments on coating and surface modification showed the following: a greater collagen synthesis appeared when gelatin-A coating was used compared to collagen-I coating conditions: Collagen matrix thickness was about 20-22um, while in collagen-I conditions this was 14um (table 6).

The effect of surface modification in terms of cross-linking and/or plasma treatment resulted in greater collagen synthesis in gelatin-A cross-linking conditions, already after ten days of culturing. At day four barely no collagen matrix was produced, or cell and matrix were loosened from the substrate, making imaging impossible (Table 7). Also in gelatin-A coated condition and prior plasma modification condition this happened at day 10.

Results experiment 1: Coating selection on silicone substrates

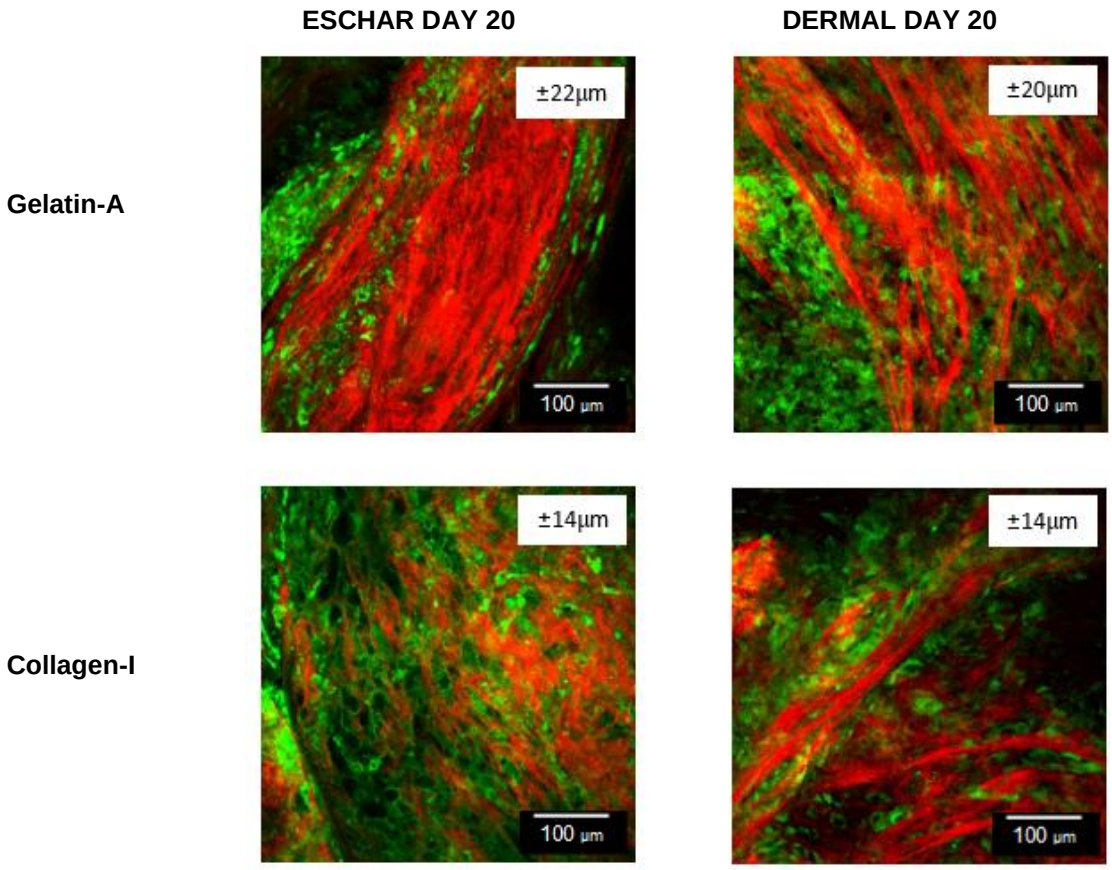

Table 6. Differences in surface modification and crosslinking on coating regimes on silicon sheet substrate. Combined 2-photon excited fluorescence image (2PEF, green) and second harmonic generation image (SHG, red) of fibroblasts and produced collagen matrix relatively, in a non-stretched culture environment on extensible silicone sheets. Thickness of collagen matrix is displayed in white (um). X is displayed for conditions where imaging was impossible.

Results experiment 2: Prior surface modification and cross-linked coating of silicone substrates

`	ESCHAR DAY 4 (donor 2)	ESCHAR DAY 10 (donor 1)	ESCHAR DAY 10 (donor 2)
Gelatin-A	X	X	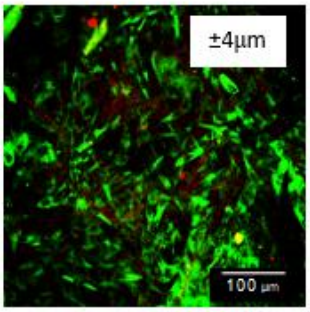
Gelatin-A crosslinked	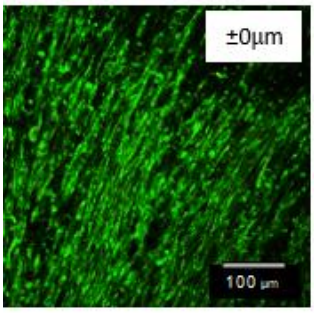	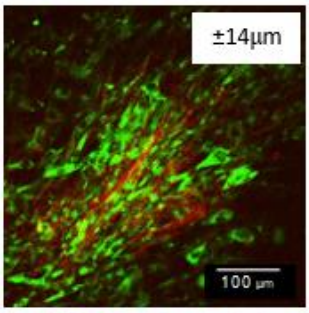	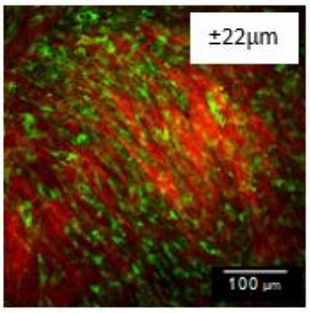
Plasma modification	X	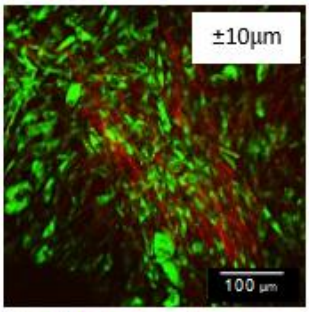	X
Plasma Gelatin Crosslinked	X	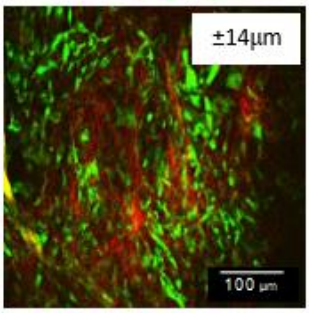	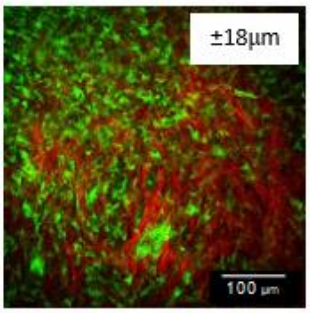

Table 7. Differences in surface modification and crosslinking on coating regimes on silicon sheet substrate. Combined 2-photon excited fluorescence image (2PEF, green) and second harmonic generation image (SHG, red) of fibroblasts and produced collagen matrix relatively, in a non-stretched culture environment on extensible silicone sheets. Thickness of collagen matrix is displayed in white (um). X is displayed for conditions where imaging was impossible.

4.3.2 Substrate characterization

For non centralized PIV analyses, strain distribution showed a larger strain at the edges of the silicone sheet, gradually decreasing towards the center (Figure 15b). Noteworthy is the lower strain indicated by the red circle. However, centralization to the middle of the pictures resulted in another strain distribution (figure 15c) in which a larger strain is showed at the site where the gooseneck of MCB1 is attached and applies an elongation in the stretch direction of the arrow, and gradually decreases towards the side where the star and thus substrates is attached to t test chamber.

Results experiment 3: Strain analysis of substrate surface

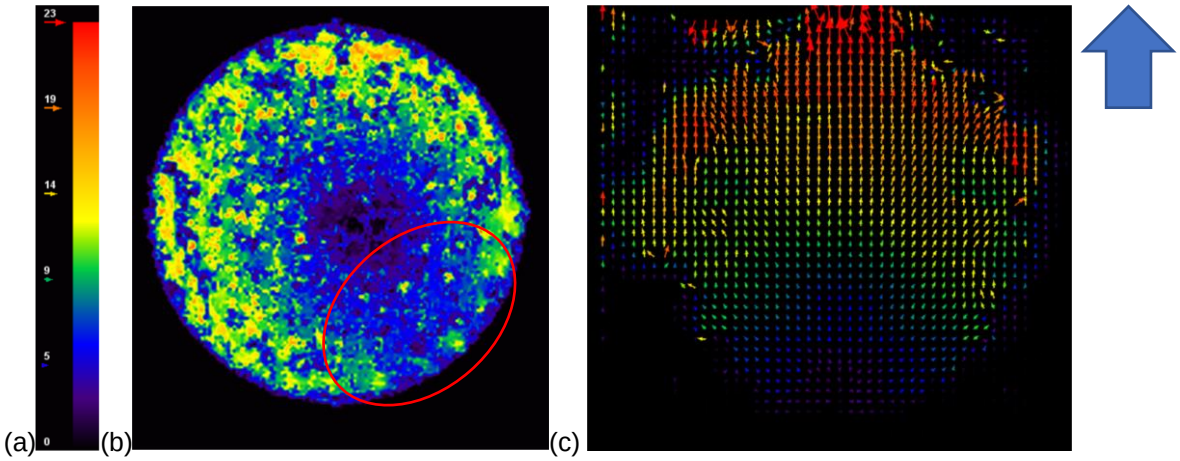

Figure 15. (a) scale graph red = high strain, blue = low strain, green/yellow = in between strain; Strain distribution with help of PIV analysis (b) magnitude plot after centralization (c) vector plot when no centralization of the images is applied. Stretch direction is visualized by the blue arrow.

Figure 16 shows a box plot of the value of the storage modulus (E') at 5.62 Hz frequency of the 4 different conditions. As can be seen storage modulus was highest for the unstretched gelatin-A crosslinked coated condition. When comparing stretched conditions to unstretched conditions, stretched conditions showed significantly higher storage moduli. Furthermore, when comparing unstretched coated conditions to unstretched non-coated conditions, coated conditions showed increased storage modulus.

Results experiment 4: Effect of cross-linked coating and stretch on stiffness of the substrate

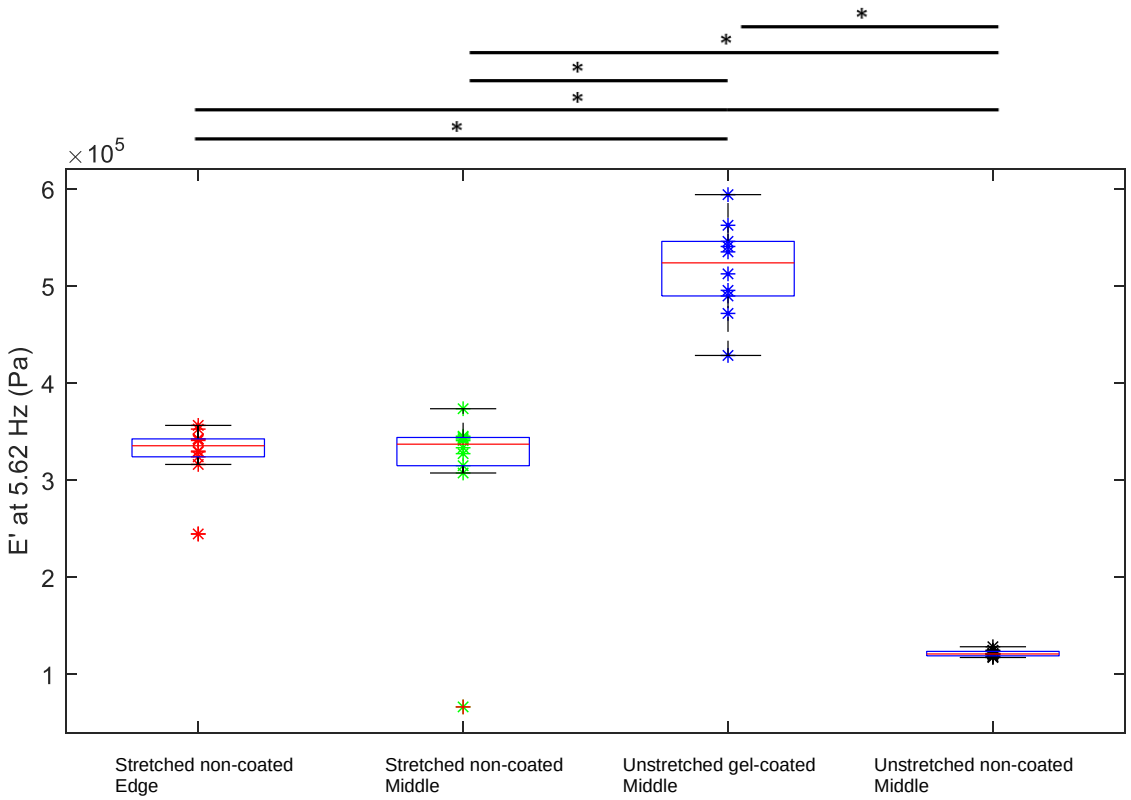

Condition	Average E' ± std (Pa)
Stretched non-coated (edge)	3.28e05 ± 0.32e05
Stretched non-coated (middle)	3.10e05 ± 0.87e05
Unstretched gel-coated (middle)	5.18e05 ± 0.48e05
Unstretched non-coated (middle)	1.21e05 ± 0.03e05

Figure 16. Effect of cross-linked gelatin-A coating (= gel-coated) and 20% stretch on storage modulus (E') of the edge and middle of the silicone substrate in stretched and non-stretched conditions. Red stripe is average, box represent 2nd and 3rd quartile, black stripes represent 1st and 4th quartile, loose stars are outliers. *p<0.5

4.3.3 Growth medium optimization

Results experiment 7: Magnitude of l-ascorbic acid stimulation

	ESCHAR DAY 20	DERMAL DAY 20
50 ug/ml	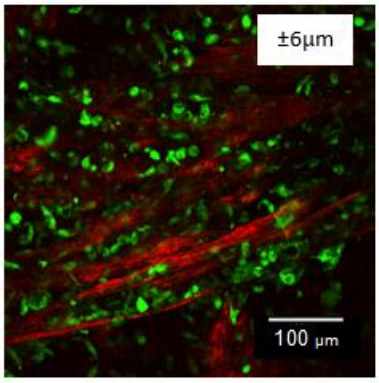	X
65 ug/ml	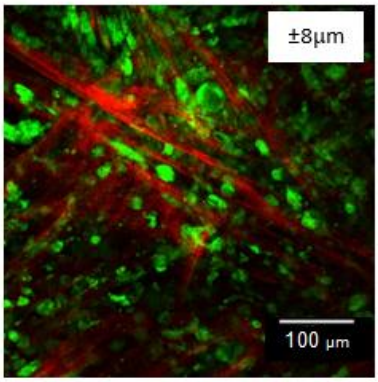	X
75 ug/ml	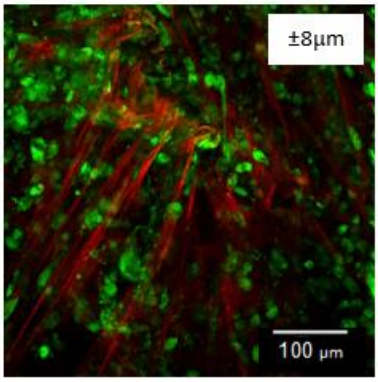	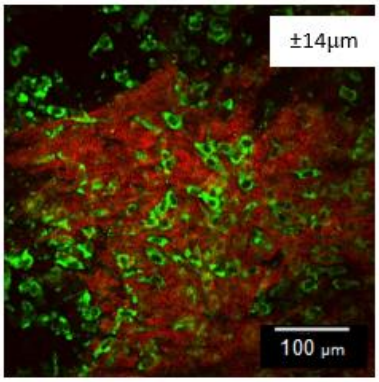

Table 8. Differences in magnitude of stimulation with l-ascorbic acid to cell cultures.
Combined 2-photon excited fluorescence image (2PEF, green) and second harmonic generation image (SHG, red) of fibroblasts and produced collagen matrix relatively, in a non-stretched culture environment on extensible silicone sheets. Thickness of collagen matrix is displayed in white (um). X is displayed for conditions where imaging was impossible.

After 21 days of culturing sufficient ECM was produced by the fibroblasts and imaging of the conditions started. In conditions where 75 ug/ml was added to the supplemented DMEM content, collagen synthesis was greatest compared to conditions where 50ug/ml or 65ug/ml was added: Collagen matrix thickness was about 8-14um, while in other conditions this was about 6um and 8um respectively (Table 8).

Results experiment 8: Growth medium selection

	ESCHAR DAY 10	DERMAL DAY 10
Supp DMEM	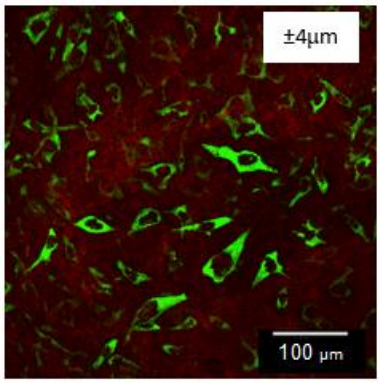	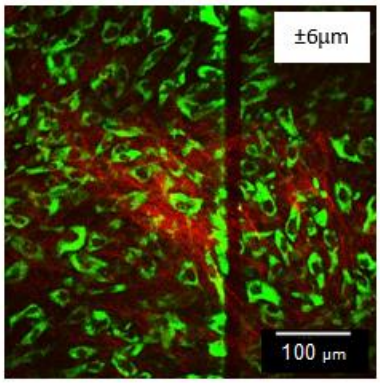
CNT-05	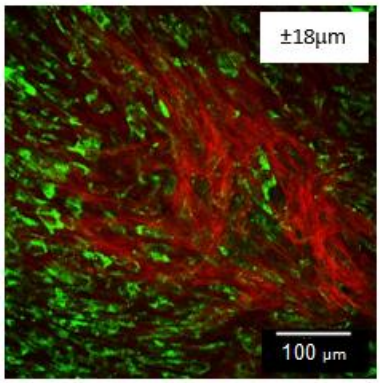	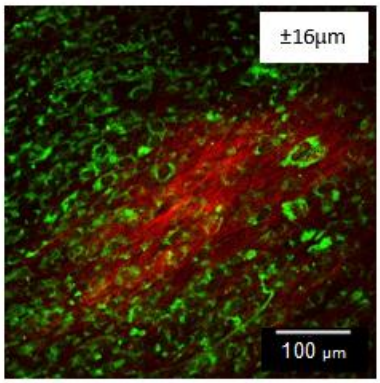
CnT-PR-ECM	X	X

Table 9. Cell cultures where supplemented DMEM (supp DMDM), CNT-05 or CnT-PR-ECM is used as growth medium in each condition. Combined 2-photon excited fluorescence image (2PEF, green) and second harmonic generation image (SHG, red) of fibroblasts and produced collagen matrix relatively, in a non-stretched culture environment on extensible silicone sheets. Thickness of collagen matrix is displayed in white (um). X is displayed for conditions where imaging was impossible.

Sufficient ECM was produced already after ten days of culturing. Using CNT-05 for growth medium for cell cultures appeared to result in a greater synthesis compared to other conditions, as can be seen in table 9. Using this growth medium, collagen matrix thickness was about 16-18um, whereas thickness after use of supplemented DMEM barely any collagen matrix was produced. In samples cultured with CnT-PR-ECM, the entire layer of cells and matrix detached from the substrate and disintegrated after 10 days, making imaging impossible.

4.4 Validation of the attained in vitro burn splinting model

During the pilot study, after ten days of culturing, results indicated that sufficient ECM was produced to make a comparison between treatment groups.
The exception was the HDF sample in dynamic stretched condition, in which barely any collagen was produced. In addition, the HDF sample in static stretched condition was detached from the substrate and disintegrated, making imaging and other analyses impossible.

No infection were detected, and only one control sample (non-stretched HDF) showed leakage of the medium culture. This sample was excluded from the experiment. Practical use of MCB1 went well in terms of simplicity of sterilization and daily culture refreshment. In addition, stretch regime was executed without difficulties. For transportation of the MCB1 and samples to a new location for imaging, original cases and covers were used to prevent leakage because chambers were then completely filled with culture medium.

Quantitative analysis of collagen synthesis and density of pilot study
In statically stretched conditions the thickness of collagen matrix of the samples synthesized by HEF was 60% greater compared to their control group (Table 10). However, in HEF dynamically stretched conditions thickness of collagen type-I matrix barely differed from the unstretched controls. In addition, static stretch conditions showed greater collagen type I matrix thickness (45%) than dynamic stretched condition.
Differences in collagen matrix thickness were observed after 10 days of culture between HDF and HEF exposed to stress and control. There, synthesis of collagen type I by hEE was 2 times thicker in unstretched conditions, and about 11 times thicker in dynamic stretched conditions.

	ESCHAR, DAY 10	DERMAL, DAY 10
Unstretched controls	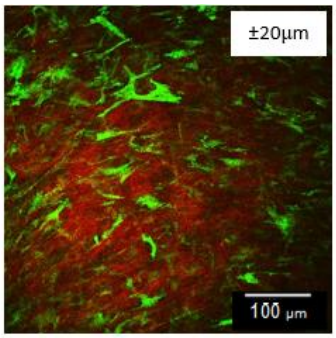	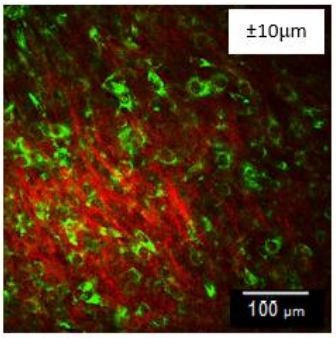
Static stretch	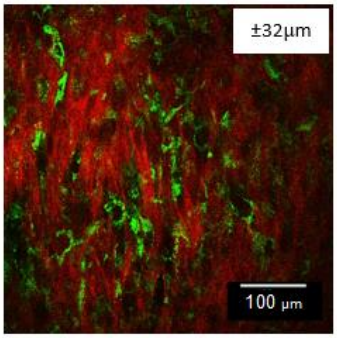	X
Dynamic stretch	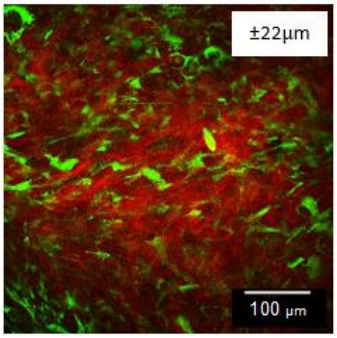	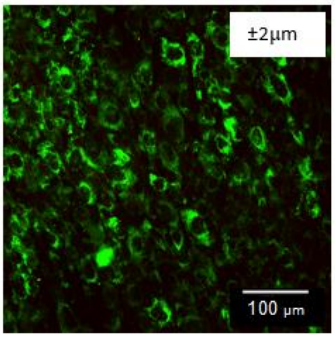

Table 10. Differences in magnitude of stimulation to cell cultures. Combined 2-photon excited fluorescence image (2PEF, green) and second harmonic generation image (SHG, red) of fibroblasts and produced collagen matrix relatively, in a non-stretched culture environment on extensible silicone sheets. Thickness of collagen matrix is displayed in white (um). X is displayed for conditions where imaging was impossible.

Collagen fiber density synthesized by HDF and HEF was greater in statically and dynamically stretched conditions, compared to the control group (Table 11). This difference was about 145% in static stretch condition and 100% in dynamic stretch condition. When comparing static stretch to dynamic stretch, in static stretch conditions collagen type I density was 23% higher in static stretched conditions.

Differences in collagen density were observed for HDF and HEF in dynamic stretched condition: density was 6 times greater for HEF than for HDF.

Condition	**%area of ROI**	
	HEF derived collagen matrix	***HDF derived collagen matrix***
Unstretched control	15.5278 ± 10.6839	14.4536 ± 7.7938
Static stretch	37.2597 ± 3.1911*	-
Dynamic stretch	30.4196 ± 3.2321*	5.0231

Table 11. Collagen density. Data are expressed as the mean ± SD. *p<0.05 compared to cell line based control group.

Quantitative analysis of collagen fiber alignment

ECM produced by statically and dynamically stretched fibroblasts showed significantly greater alignment ($p<0.05$), compared to the non-stretched control group (Table 12). No significant differences in alignment were observed between HDF and HEF in each condition. Also no significant differences were seen in alignment between static and dynamic stretch.

Condition	***Alignment coefficient***	
	HEF derived collagen fiber (Mean ± SD)	***HDF derived collagen fiber (Mean ± SD)***
Non-stretch	0.33 ± 0.10	0.39 ± 0.09
Static stretch	0.53 ± 0.12*	-
Dynamic stretch	0.50 ± 0.28*	0.3

Table 12. Alignment of collagen fibers produced by HEF and HDF after 10 days of culturing in three different conditions: non-stretched, static stretched and dynamic stretch.. *p<0.05 compared to cell line based control group.

Double immunostaining

Results showed that double immunostaining did not manage. However, in contrast to a-SMA, collagen type I could be identified in single immunostaining in both HEF and HDF cell cultures. Negative controls confirmed successfully immunostaining. Collagen-I fibers seemed to concentrate in the area surrounding the fibroblasts (Figure 16). In addition, the figures show that collagen type I staining in HEF was stronger than in HDF.

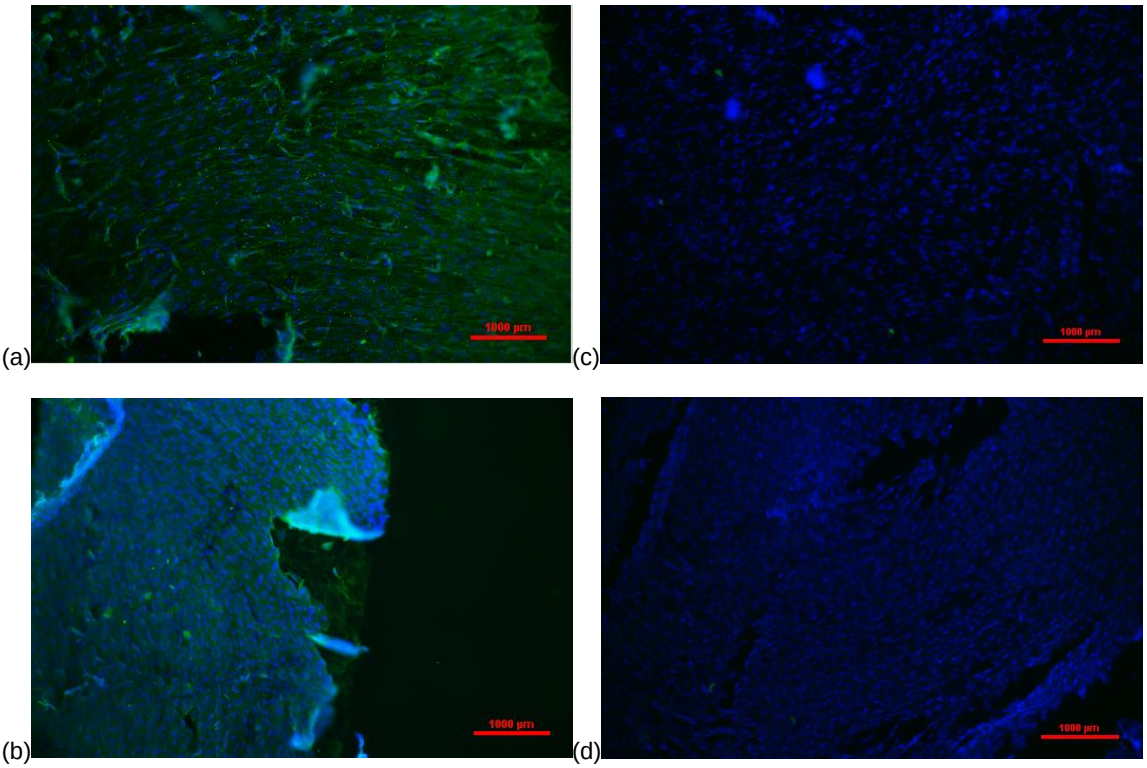

Figure 16. Collagen type 1 visualization using Streptavidin-AF488 (green) in conditions where HEF (a) and HDF (b) are dynamically stretched and visualized using DAPI (blue); (c,d) col1 negative controls.

Gene expression rate of a-SMA

qPCR showed that after ten days, non-stretched fibroblasts' expression of a-SMA was increased. Furthermore, after ten days a-SMA gene expression rate was greater in the condition where HDF were cultured than in the condition where HEF were cultured (Figure 17).

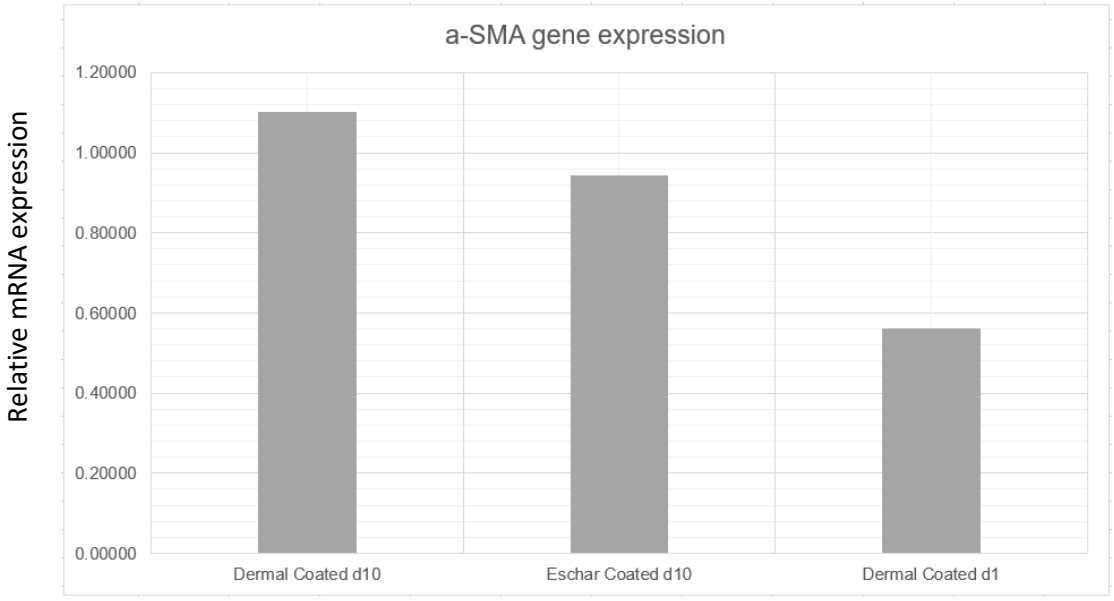

Figure 17. Relative mRNA expression rates of a-SMA on day 1 (d1) and day 10 (d10) in non-stretched eschar and dermal cell cultures on coated standard culture dishes.

5. Conclusion and discussion

The aim of the present study was to design a suitable in vitro model of mechanotransduction in burn wounds, to investigate the molecular effects of burn splinting in vitro. Three chronological sub-goals were defined to achieve the eventual burn wound splinting model: (1) formulating a suitable mechanical stress protocol (2) select a system that enables mechanical stress of extensible substrates that facilitate the growth of fibroblasts and their derived ECM and (3) create and optimize conditions to culture fibroblasts on an extensible substrate. To successfully reach these goals, the current literature on this subject was evaluated and comparative experiments were executed.

The final in vitro model includes a clinically relevant stress protocol, a practical device capable of executing this protocol while providing optimal culture conditions for dermal cells. The MCB1 stretching apparatus provided by ADBC was modified to fulfill all requirements, including compatibility with analytical devices such as microscopes and micro indenters. An extensible silicone culture dish was custom made to fit the stretching device. Cross-linked gelatin was selected as an optimal substrate coating, while CNT-05 growth medium supplemented with vitamin C was found to be the optimal culture medium.

In comparison with related studies in literature, the model constitutes a substantial leap forward. In these studies, it was shown that in general mechanical stretch stimulated fibroblasts' synthesis of collagen[36,43,51,55], and increased collagen fiber alignment[42]. However, these analyses were done in highly processed histopathology slides. In situ, or even in vitro imaging by means of SHG microscopy allows three dimensional analysis of the produced ECM, without processing artefacts.
Furthermore, elevated levels of a-SMA gene expression were found in certain cell types, leading authors to deduce prematurely that scar contracture rates will be higher. Certainly, without measuring matrix stiffness, no such extrapolation can be me made. Including micro-indentation analysis of matrix stiffening thus increases the translational value of the mode.
No studies were found that specifically evaluated mechanotransducive effects in a burn wound model. By using burn-derived eschar fibroblasts, this model more accurately mimics the distinct features that result in the particularly debilitating scars after burn wounds.
Furthermore, in contrast to previous studies in which motivations for parameters settings like magnitude of strain, frequency and duration were often not specified or based on general approximations, the selected stretch protocol in this study was based on physiotherapeutic treatments regimens used in burn centers daily. The rational for the stretching parameters makes the model truly clinically relevant, in the absence of concrete evidence from experimental studies.

This study has some limitations.

Although micro indentation-based quantification of matrix stiffness was not possible in the samples due to technical limitations of the micro indenter, its application in this model will provide invaluable information about adaptations in matrix function under stress.

Another limitation is that strain varies depending on the location on the substrate. Furthermore, the effective strain exerted on cells cultured in this method is not known except for the edges. This issue is similar to several studies in literature, using a popular stretching device[36]. The implication of this issue is that the obtained results may vary depending on localization, possibly resulting in a false comparison when comparing outcome measures on different locations of the substrate. In experiment 3 an attempt was done to identify strain analysis of rubber silicone substrates. However, errors can occur which can be due to inaccuracy of the software in tracking the markers. When looking at the deformation of the silicone sheets in practical terms, strain distribution resulted when no centralization of the images was conducted seems more plausible. In order to draw firm conclusions, a finite element analysis could be carried out in future studies.

In addition, the strain exerted on the substrate results in stiffening of the substrate. Sun et al. (2018) showed that this substrate stiffening in itself results in higher proliferation and differentiation of cultured cells[85]. Moreover, based on literature study outcomes, proliferation is also influenced by stretching the samples[49]. Therefore, it is difficult to determine the actual cause of a potential difference in outcome, when both substrate stiffness, and actual strain exerted on the cells have similar effects.

Another limitation of the present model is the small sample size of the comparative experiments. Validation of the designed in vitro burn splinting model showed that HEFs produced sufficient ECM for measurement, in contrast to HDFs which barely produced ECM after ten days of culturing. Although similar experiments with HDFs showed more than ample collagen production on a similar time scale. This illustrates the effect of donor variability and aging of cell cultures used for these experiments. Repeat measurements are invaluable to produce results that are significant, reproducible, and applicable to the clinic.

Nonetheless, based on the pilot study both dynamic and static stretched HEF showed a trend towards thicker, denser collagen matrices compared to unstretched conditions. These collagen fibers also showed a greater degree of alignment. However, no definitive conclusions can be drawn since sample size is limited.

Future research can focus on determinations of optimal strain, frequency and duration of stretching experiments that produces optimal mechanical and biochemical responses for each particular applications.

Translating this model to the clinical situation may seem difficult; the model excludes systemic variables such as circulation, nutrition through blood flow, and inflammatory mediators[33], which all contribute to the clinical outcome of burn wound healing and recovery. It is therefore hard to accurately mimic the pathological conditions of hypertrophic scarring and wound healing. However, all the local components including ECM and viable cells are present in the samples, and therefore future findings using this model provide a simplified principle of the nature of biological processes of scarring after burn injuries, which

favor insight into the pathogenic mechanism of scarring and further investigation for clinical prevention and treatment in this debilitating process.

Based on comparative experiments, validation of the model and after consideration of the model's limitations, we may conclude that this design is a promising model to investigate the effects of splinting strategies on burn wounds.

References

1. Dokter J, Vloemans AF, Beerthuizen GI, et al. Epidemiology and trends in severe burns in the Netherlands. *Burns*. 2014;40(7):1406-1414.
2. Leavitt T, Hu MS, Marshall CD, Barnes LA, Lorenz HP, Longaker MT. Scarless wound healing: finding the right cells and signals. *Cell Tissue Res*. 2016;365(3):483-493.
3. Koppenol DC, Vermolen FJ. Biomedical implications from a morphoelastic continuum model for the simulation of contracture formation in skin grafts that cover excised burns. *Biomech Model Mechanobiol*. 2017;16(4):1187-1206.
4. Schouten HJ, Nieuwenhuis MK, Van Zuijlen PPM. A review on static splinting therapy to prevent burn scar contracture: do clinical and experimental data warrant its clinical application? *Burns*. 2012;38(1):19-25.
5. Zhang YT, Li-Tsang CW, Au RK. A Systematic Review on the Effect of Mechanical Stretch on Hypertrophic Scars after Burn Injuries. *Hong Kong J Occup Ther*. 2017;29:1-9.
6. Chiang RS, Borovikova AA, King K, et al. Current concepts related to hypertrophic scarring in burn injuries. *Wound Repair Regen*. 2016;24(3):466-477.
7. Tan J, Wu J. Current progress in understanding the molecular pathogenesis of burn scar contracture. *Burn Trauma*. 2017;5(1):14.
8. Nisanci M, Sahin I, Guzey S. An extraordinary case of axillary contracture: Trapped healthy skin and its adnexes under contracted scar. *Int Surg*. 2014;99(4):442-446.
9. Aziz J, Shezali H, Radzi Z, et al. Molecular Mechanisms of Stress-Responsive Changes in Collagen and Elastin Networks in Skin. *Skin Pharmacol Physiol*. 2016;29(4):190-203.
10. Couet J, Shengwen L, Okamoto T, Scherer PE, Lisanti MP. Molecular and Cellular Biology of Caveolae. *Trends Cardiovasc Med*. 1997;7(4):103-110.
11. Duscher D, Maan ZN, Wong VW, et al. Mechanotransduction and fibrosis. *J Biomech*. 2014;47(9):1997-2005.
12. Doyle AD, Yamada KM. Mechanosensing via cell-matrix adhesions in 3D microenvironments. *Exp Cell Res*. 2016;343(1):60-66.
13. Verhaegen PD, Van Zuijlen PP, Pennings NM, Van Marle J, Niessen FB, Van Der Horst, C. M. Middelkoop E. Differences in collagen architecture between keloid, hypertrophic scar, normotrophic scar, and normal skin: An objective histopathological analysis. *Wound Repair Regen*. 2009;17(5):649-656.
14. Sun Z, Williams GM. Skin Wound Healing: Skin Regeneration With Pharmacological Mobilized Stem Cells. In: *In Situ Tissue Regeneration*. ; 2016:345-368.
15. Rosenberg L. *Enzymatic Debridement of Burn Wounds*.; 2012.
16. Suda S, Williams H, Medbury HJ, Holland AJ. A Review of Monocytes and Monocyte-Derived Cells in Hypertrophic Scarring Post Burn. *J Burn Care Res*. 2016;37(5):265-272.
17. Reinke JM, Sorg H. Wound repair and regeneration. *Eur Surg Res*. 2012;49(1):35-43.
18. Barnes LA, Marshall CD, Leavitt T, et al. Mechanical Forces in Cutaneous Wound Healing: Emerging Therapies to Minimize Scar Formation. *Adv Wound Care*. 2018;7(2):47-56.
19. Zhang Y, Lin Z, Foolen J, et al. Disentangling the multifactorial contributions of fibronectin, collagen and cyclic strain on MMP expression and extracellular matrix remodeling by fibroblasts. *Matrix Biol*. 2014;40:62-72.
20. Van De Water L, Varney S, Tomasek JJ. Mechanoregulation of the Myofibroblast in Wound Contraction, Scarring, and Fibrosis: Opportunities for New Therapeutic Intervention. *Adv Wound Care*. 2013;2(4):122-141.
21. Hinz B. Myofibroblasts. *Exp Eye Res*. 2016;142:56-70.
22. Bildyug N. Matrix metalloproteinases: An emerging role in regulation of actin microfilament system. *Biomol Concepts*. 2016;7(5-6):321-329.
23. Van Den Bogaerdt AJ, Van Der Veen VC, Van Zuijlen PPM, et al. Collagen cross-linking by adipose-derived mesenchymal stromal cells and scar-derived mesenchymal cells: Are

mesenchymal stromal cells involved in scar formation? *Wound Repair Regen*. 2009;17(4):548-558.
24. Hinz B. The extracellular matrix and transforming growth factor-β1: tale of a strained relationship. *Matrix Biol*. 2015;47:54-65.
25. Werdin F, Tenenhaus M, Becker M, Rennekampff H. Healing Time Correlates With the Quality of Scaring: Results From a Prospective Randomized Control Donor Site Trial. *Dermatologic Surg*. 2018;44(4):521-527.
26. Parashar A, Atla K, Sharma RK. Static splinting in burns. *Burn J Int Soc Burn Inj*. 2013;39(1):190.
27. Richard, Reg and RSW. Splinting strategies and controversies. *J Burn Care Rehabil*. 2005;26(5):392-396.
28. Ferro KJ, Morgano SM, Driscoll CF, et al. *The Glossary of Prosthodontic Terms*.
29. Kwan MW, Ha KW. Splinting programme for patients with burnt hand. *Hand Surg*. 2002;7(2):231-241.
30. Patton KT, Thibodeau GA. Mosby's Handbook of Anatomy & Physiology. *Elsevier Heal Sci*. 2014.
31. Walraven M. Cellular and molecular mechanisms involved in scarless wound healing in the fetal skin. 2016:1-144.
32. Veltman ES, Doornberg JN, Eygendaal D, van den Bekerom MP. Static progressive versus dynamic splinting for posttraumatic elbow stiffness: a systematic review of 232 patients. *Arch Orthop Trauma Surg*. 2015;135(5):613-617.
33. Fröhlich E, Salar-Behzadi S. Toxicological assessment of inhaled nanoparticles: Role of in vivo, ex vivo, in vitro, and in Silico Studies. *Int J Mol Sci*. 2014;15(3):4795-4822.
34. Beacham DA, Amatangelo MD, Cukierman E. Preparation of extracellular matrices produced by cultured and primary fibroblasts. *Curr Protoc cell Biol*. 2006;33(1):10-19.
35. Cuerrier C, Pelling A. Cells, forces, and the microenvironment. 2015.
36. Balestrini, J. L., & Billiar KL. Equibiaxial cyclic stretch stimulates fibroblasts to rapidly remodel fibrin. *J Biomech*. 2006;39(16):2983-2990.
37. Kreutzer J, Ikonen L, Hirvonen J, Pekkanen-Mattila M, Aalto-Setälä K, Kallio P. Pneumatic Cell Stretching System for Cardiac Differentiation and Culture. *Med Eng Phys*. 2014;36(4):496-501.
38. Neidlinger-Wilke C, Grood E, Claes L, Brand R. Fibroblast orientation to stretch begins within three hours. *J Orthop Res*. 2002;20(5):953-956.
39. Nishimura K, Blume P, Ohgi S, Sumpio BE. Effect of different frequencies of tensile strain on human dermal fibroblast proliferation and survival. *Wound Repair Regen*. 2007;15(5):646-656.
40. Reichenbach M, Reimann K, Reuter H. Gene expression in response to cyclic mechanical stretch in primary human dermal fibroblasts. *Genomics data*. 2014;2:335-339.
41. Rolin G, Binda D, Tissot M, et al. In vitro study of the impact of mechanical tension on the dermal fibroblast phenotype in the context of skin wound healing. *J Biomech*. 2014;47(14):3555-3561.
42. Shikano K, Chiba K, Miyata S. Response of Human Skin Fibroblasts to Mechanical Stretch in Wound Healing Process Analyzed Using a Three-Dimensional Culture Model. *Adv Biomed Eng*. 2015;4(0):170-178.
43. Syedain Z, Biomechanics RT-J of, 2011 U. TGF-β1 diminishes collagen production during long-term cyclic stretching of engineered connective tissue: implication of decreased ERK signaling. *J Biomech*. 2011;44(5):848-855.
44. Tokuyama E, Nagai Y, Takahashi K, One YK-P, 2015 U. Mechanical stretch on human skin equivalents increases the epidermal thickness and develops the basement membrane. *PloS*. 2015;10(11):1-12.
45. Wang JHC, Grood ES. The strain magnitude and contact guidance determine orientation response of fibroblasts to cyclic substrate strains. *Connect Tissue Res*. 2000;41(1):29-36.
46. Wang Z, Fong KD, Phan TT, Lim IJ, Longaker MT, Yang GP. Increased transcriptional response to mechanical strain in keloid fibroblasts due to increased focal adhesion complex formation. *J Cell Physiol*. 2006;206(2):510-517.
47. Weidenhamer NK, Tranquillo RT. Influence of Cyclic Mechanical Stretch and Tissue Constraints on Cellular and Collagen Alignment in Fibroblast-Derived Cell Sheets. *Tissue Eng*. 2013;19(5):386-395.
48. Du Q cui, Zhang D zun, Chen X juan, Lan-Sun G, Wu M, Xiao W lin. The Effect of p38MAPK on Cyclic Stretch in Human Facial Hypertrophic Scar Fibroblast Differentiation. *PLoS One*. 2013;8(10).
49. Huang C, Miyazaki K, Akaishi S. Biological effects of cellular stretch on human dermal

fibroblasts. *J Plast Reconstr Aesthetic Surg*. 2013;66(12):351-361.
50. Ishise H, Larson B, Hirata Y, Fujiwara T. Hypertrophic scar contracture is mediated by the TRPC3 mechanical force transducer via NFkB activation. *Sci Rep*. 2015;5:11620.
51. Jiang M, Qiu J, Zhang L. Changes in tension regulates proliferation and migration of fibroblasts by remodeling expression of ECM proteins. *Exp Ther Med*. 2016;12(3):1542-1550.
52. Kessler D, Dethlefsen S, Haase I, et al. Fibroblasts in Mechanically Stressed Collagen Lattices Assume a “Synthetic” Phenotype. *J Biol Chem*. 2001;276(39):36575-36585.
53. Kim M, Shin DW, Shin H, Noh M, Shin JH. Tensile stimuli increase nerve growth factor in human dermal fibroblasts independent of tension-induced TGFβ production. *Exp Dermatol*. 2013;22(1):72-74.
54. Kuang R, Wang Z, Xu Q, Liu S, Zhang W. Influence of mechanical stimulation on human dermal fibroblasts derived from different body sites. *Int J Clin Exp Med*. 2015;8(5):7641-7647.
55. Kuang R, Wang Z, Xu Q, Cai X. Exposure to varying strain magnitudes influences the conversion of normal skin fibroblasts into hypertrophic scar cells. *Ann Plast Surg*. 2016;76(4):388-393.
56. Brown TD, Bottlang M, Pedersen DR, Banes AJ. Development and experimental validation of a fluid/structure-interaction finite element modelof a vacuum-driven cell culture mechanostimulus system. *Comput Methods Biomech Biomed Engin*. 2000;3(1):65-78.
57. Davidson DBM and MW. Two-Photon Excitation Fluorescence Microscopy. In: *Fundamentals of Light Microscopy and Electronic Imaging*. ; 2012:307-329.
58. Benninger RK, Piston DW. Two-photon excitation microscopy for unit 4.11 the study of living cells and tissues. *Curr Protoc Cell Biol*. 2013;59(1):4-11.
59. Pena A-M, Olive C, Michelet J-F, et al. Multiphoton microscopy of engineered dermal substitutes: assessment of 3D collagen matrix remodeling induced by fibroblasts contraction. *J Biomed Opt*. 2010;15(5).
60. Mostaço-Guidolin L, Rosin N, Hackett TL. Imaging collagen in scar tissue: Developments in second harmonic generation microscopy for biomedical applications. *Int J Mol Sci*. 2017;18(8):1772.
61. Strupler, M., Pena, A. M., Hernest, M., Tharaux, P. L., Martin, J. L., Beaurepaire, E., & Schanne-Klein MC. Second harmonic imaging and scoring of collagen in fibrotic tissues. *Opt Express*. 2007;15(7):4054-4065.
62. Bancelin S, Nazac A, Ibrahim BH, et al. Determination of collagen fiber orientation in histological slides using Mueller microscopy and validation by second harmonic generation imaging. *Opt Express*. 2014;22(19):22561.
63. Xue M, Jackson CJ. Extracellular Matrix Reorganization During Wound Healing and Its Impact on Abnormal Scarring. *Adv Wound Care*. 2015;4(3):119-136.
64. Y. Liu, A. Keikhosravi, G. S. Mehta CRD and KW, Eliceiri. Methods for Quantifying Fibrillar Collagen Alignment. *Pathobiol Cancer Regimen-Related Toxicities*. 2013:167-186.
65. Owen GR, HäKkinen L, Wu C, Larjava H. A reproducible technique for specific labeling of antigens using preformed fluorescent molecular IgG-F(ab’)2 complexes from primary antibodies of the same species. *Microsc Res Tech*. 2010;73(6):623-630.
66. Hinz B, Celetta G, Tomasek JJ, Gabbiani G, Chaponnier C. Alpha-smooth muscle actin expression upregulates fibroblast contractile activity. *Mol Biol Cell*. 2001;12(9):2730-2741.
67. Nolan T, Huggett J, Sanchez E. Good Practice Guide for the Application of Quantitative PCR (qPCR). *Natl Meas Syst*. 2013:50.
68. Krzystek-Korpacka M, Diakowska D, Bania J, Gamian A. Expression stability of common housekeeping genes is differently affected by bowel inflammation and cancer: Implications for finding suitable normalizers for inflammatory bowel disease studies. *Inflamm Bowel Dis*. 2014;20(7):1147-1156.
69. Han YL, Ronceray P, Xu G, et al. Cell contraction induces long-ranged stress stiffening in the extracellular matrix. *Proc Natl Acad Sci*. 2018;115(16):4075-4080.
70. Silver FH, Landis WJ. Viscoelasticity, energy storage and transmission and dissipation by extracellular matrices in vertebrates. In: *Collagen*. Springer US; 2008:133-154.
71. Antonovaite N, Beekmans S V., Hol EM, Wadman WJ, Iannuzzi D. Regional variations in stiffness in live mouse brain tissue determined by depth-controlled indentation mapping. *Sci Rep*. 2018;8(1):1-11.
72. Marrese M, Antonovaite N, Nelemans BKA, Smit TH, Iannuzzi D. Micro-indentation and optical coherence tomography for the mechanical characterization of embryos: Experimental setup and measurements on fixed chicken embryos. *bioRxiv*. 2019.
73. Haji-Saeid M, Sampa MHO, Chmielewski AG. Radiation treatment for sterilization of packaging

materials. *Radiat Phys Chem*. 2007;76(8-9):1535-1541.
74. Arora M. Cell Culture Media: A Review. *Mater Methods*. 2013;3(175):24.
75. Pavel M, Renna M, Park SJ, et al. Contact inhibition controls cell survival and proliferation via YAP/TAZ-autophagy axis. *Nat Commun*. 2018;9(1):2961.
76. J Paul. Cell and tissue culture. *Cell tissue Cult (4th Ed*. 1970.
77. Leivo J, Kartasalo K, Kallio P, et al. A durable and biocompatible ascorbic acid-based covalent coating method of polydimethylsiloxane for dynamic cell culture. *J R Soc Interface*. 2017;14(132).
78. Wong I, Ho CM. Surface molecular property modifications for poly(dimethylsiloxane) (PDMS) based microfluidic devices. *Microfluid Nanofluidics*. 2009;7(3):291-306.
79. Halldorsson S, Lucumi E, Gómez-Sjöberg R, Fleming RMT. Advantages and challenges of microfluidic cell culture in polydimethylsiloxane devices. *Biosens Bioelectron*. 2015;63:218-231.
80. Safaeijavan R, Soleimani M, Divsalar A, Eidi A. Biological behavior study of gelatin coated PCL nanofiberous electrospun scaffolds using fibroblasts. *J Paramed Sci*. 2014;5(1):67-73.
81. Grover CN, Gwynne JH, Pugh N, et al. Crosslinking and composition influence the surface properties, mechanical stiffness and cell reactivity of collagen-based films. *Acta Biomater*. 2012;8(8):3080-3090.
82. Nair TM, Kumaran MG, Unnikrishnan G, Pillai VB. Dynamic mechanical analysis of ethylene-propylene-diene monomer rubber and styrene-butadiene rubber blends. *J Appl Polym Sci*. 2009;112(1):72-81.
83. Ai H, Mills DK, Jonathan AS, Jones SA. Gelatin-glutaraldehyde cross-linking on silicone rubber to increase endothelial cell adhesion and growth. *Vitr Cell Dev Biol - Anim*. 2002;38(9):487-492.
84. Lai JY, Lin YY, Denq YL, Shyu SS, Chen JK. Surface modification of silicone rubber by gas plasma treatment. *J Adhes Sci Technol*. 1996;10(3):231-242.
85. Sun M, Chi G, Li P, et al. Effects of matrix stiffness on the morphology, adhesion, proliferation and osteogenic differentiation of mesenchymal stem cells. *Int J Med Sci*. 2018;15(3):257-268.
86. Engler AJ, Sen S, Sweeney HL, Discher DE. Matrix Elasticity Directs Stem Cell Lineage Specification. *Cell*. 2006;126(4):677-689.
87. Anderson SML, McLean WHI, Elliot RJ. The effects of ascorbic acid on collagen synthesis by cultured human skin fibroblasts. 1991.
88. Boyera N, Galey I, Bernard BA. Effect of vitamin C and its derivatives on collagen synthesis and cross- linking by normal human fibroblasts. *Int J Cosmet Sci*. 1998;20(3):151-158.
89. Soltow QA, Lira VA, Betters JL. Nitric oxide regulates stretch-induced proliferation in C2C12 myoblasts. *J Muscle Res Cell Motil*. 2010;31(3):215-225.
90. Arnoczky SP, Tian T, Lavagnino M, Gardner K, Schuler P, Morse P. Activation of stress-activated protein kinases (SAPK) in tendon cells following cyclic strain: The effects of strain frequency, strain magnitude, and cytosolic calcium. *J Orthop Res*. 2002;20(5):947-952.
91. Lindahl GE, Chambers RC, Papakrivopoulou J, et al. Activation of fibroblast procollagen α1(I) transcription by mechanical strain is transforming growth factor-β-dependent and involves increased binding of CCAAT-binding factor (CBF/NF-Y) at the proximal promoter. *J Biol Chem*. 2002;277(8):6153-6161.
92. Lee JN, Jiang X, Ryan D, Whitesides GM. Compatibility of mammalian cells on surfaces of poly(dimethylsiloxane). *Langmuir*. 2004;20(26):11684-11691.

Appendix

Appendix 1: Abbreviations

ADBC	Association of Dutch Burn Centre
a-SMA	alpha smooth muscle-actin
ECM	Extracellular matrix
FBS	fetal bovine serum
HDF	Human dermal fibroblasts
HEF	Human eschar fibroblasts
HS	Hypertrophic scars
KF	keloid fibroblasts
KS	Keloid scars
MCB1	MechanoCulture B1
OCT	optical coherence tomography
PDMS	polydimethylsiloxaan
PLA	polylactic acid
PMMMA	polymethyl methacrylate
PVC	polyvinylchloride
qPCR	Quantitative polymerase chain reaction
ROI	Region of interest
SHG	second-harmonic generation
TGFB1	Transforming growth-factor beta-1
2PEF	Two Photon Excited Fluorescence

Appendix 2: A protocol to study the Cellular Effects of Mechanical Stretch on Fibroblasts' derived matrices in Normal Skin vs Burns with help of an in vitro model.

Cell culture

1. Start with a semi-confluent (80% confluent) culture of primary fibroblastic cells in 18 ml confluent medium (DMEM) containing 1% peniciline/streptomycine (5mL) (10.000 units/ml), 10% fetal calf serum (FCS) (50 mL) and 1% glutamine (5 mL) (200 mM 100%) in a 75 cm2 culture flasks; aspirate the culture medium and discard by rinsing with 10 ml DPBS− pre-heated at 37°C and aspirate.
2. Rinse the cell layer briefly with 2 ml 0.25% trypsin/0.03% EDTA (trypsin/EDTA), pre-heated at 37°C, wait for 5 minutes at 37°C and observe under an inverted microscope at room temperature until the cells have started to detach from the culture dish (1 to 3 min). Than gently aspirate off the solution.
3. Collect the cells in 10 ml of confluent medium with supplemented medium.

Preparation of silicone sheets

4. Prepare flexible circular-shaped PDMS (Sylgard 184, Dow Corning, USA) sheets of 25 mm outer-diameter and 0.8 mm thick, by combining a silicone elastomer prepolymer (base) and a cross-linker (curingagent) at a mixing ratio of 15:1 (weight ratio).
5. Place the mixture in a vacuum for 20 min to remove air bubbles formed during the mixing and trapped in the uncured liquid silicone.
6. Cast the mixture to a mold. And cure in an oven (Binder GmbH, Tuttlingen,Germany) at 65◦C for 4h. Sterilize silicone substrates by putting it in 75% ethanol solution for one day.
7. Sterilize framework with attached silicone sheet by putting it in 75% ethanol solution for one day. Sterilize other parts of the MCB1 by autoclaving in 20 minutes at 121˚C.
8. Puncture-mount the silicone sheets with its frame to the ring of the inferior part of the MCB1 framework

Coating the silicone sheets

9. Prepare a gelatin-A from porcine skin powder (Sigma) solution by dissolving 2% gelatin powder in PBS. Sterilize the gelatin solution by heating the solution in a bath with temperature at 37˚C. When dissolved, filter it.
10. Add 2 ml of 2% gelatin to the silicone substrate surface functioning as culture dish and incubate for 1 hr at 37°C.
11. Aspirate gelatin and fill chamber with 2 ml DPBS+.
12. Aspirate DPBS+ and add 2 ml of 1% glutaraldehyde (pre-diluted in DPBS+) to each silicone sheet and incubate 30 min at room temperature.
13. Wash culture dishes three times for 5 min each using 3 ml of DPBS+.
14. Add 2 ml of 1 M ethanolamine to each coverslip (or dish) and incubate 30 min at room temperature.
15. Aspirate DPBS+ from dishes and replace and fill chamber with culture medium and maintain at 37°C with 5% CO2 in a closed bath. If the medium appears purple (signifying basic pH), repeat step 15 to remove all traces of ethanolamine.

Cell seeding of the coated silicone sheets

16. Collect cells from flasks (from step 3), count cells and dilute to a final concentration of 2.5 × 10^5 cells/ml in supplemented medium.
17. Aspirate medium (from step 15) and seed 5 ×10^5 cells in 2 ml of matrix medium per sheet.
18. Fill chamber with supplemented DMEM and maintain cells on silicon at 37°C in humidified atmosphere in static conditions with 5% CO2 and culture for 24 hours before applying mechanical stress.
19. After 12-18 hr, carefully aspirate the medium from cells and replace with fresh matrix medium containing 75 µg/ml of ascorbic acid. This is day 0.

20. Ascorbic acid rapidly degrades in culture, hence changing medium with freshly made matrix medium every 24 hrs by removing half of the media volume and replenishing it with fresh media, containing 150 µg/ml ascorbic acid.

Applying mechanical stress to the silicone sheets

21. Start the stretch regime by applying the biaxial mechanical stress regimes to the silicone sheets.